

General Disclaimer

One or more of the Following Statements may affect this Document

- This document has been reproduced from the best copy furnished by the organizational source. It is being released in the interest of making available as much information as possible.
- This document may contain data, which exceeds the sheet parameters. It was furnished in this condition by the organizational source and is the best copy available.
- This document may contain tone-on-tone or color graphs, charts and/or pictures, which have been reproduced in black and white.
- This document is paginated as submitted by the original source.
- Portions of this document are not fully legible due to the historical nature of some of the material. However, it is the best reproduction available from the original submission.

GRUMMAN AEROSPACE CORPORATION

(NASA-CR-171289) THE GROWTH OF METASTABLE
PERITECTIC COMPOUNDS Final Report, third
year (Grumman Aerospace Corp.) 58 p
HC A04/MF A01

N85-15824

CSCL 11D

Unclas
13415

G3/24

RESEARCH & DEVELOPMENT CENTER

Third Year Final Report on NASA Contract NAS8-32998

REPORT RE-692

THE GROWTH OF METASTABLE PERITECTIC COMPOUNDS

DECEMBER 1984

prepared by

Ronald G. Pirich
Materials and Structural Mechanics

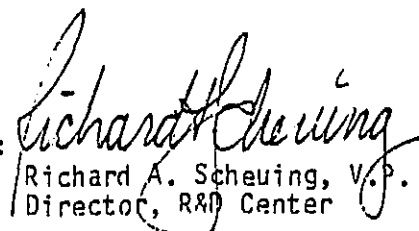
Research and Development Center
Grumman Aerospace Corporation
Bethpage, New York 11714

prepared for

National Aeronautics and Space Administration
George C. Marshall Flight Center
Marshall Space Flight Center
Alabama 35812

This report was prepared as an account of work sponsored by an agency of the United States Government. Neither the United States nor any agency thereof, nor any of their employees, make any warranty, expressed or implied, or assumes any legal liability or responsibility for any third party's use or the results of such use of any information, apparatus, product, or process disclosed in this report, or represents that its use by such third party would not infringe privately owned rights.

Approved by:


Richard A. Scheuing, V.P.
Director, R&D Center

CONTENTS

<u>Section</u>	<u>Page</u>
ABSTRACT	ix
INTRODUCTION	1
EXPERIMENTAL PROCEDURES	7
Sample Preparation	7
Experimental Composition/Test Matrix	10
Directional Solidification Processing	10
Microstructural & Microchemical Characterization	12
Magnetic Property Characterization	16
RESULTS & DISCUSSIONS	17
General Observations.	17
$\text{Sm}_2\text{Co}_{17}/\text{Co}$ Eutectic	17
$\text{SmCo}_5/\text{Sm}_2\text{Co}_{17}$ Peritectic	27
Al-Mn System	30
SUMMARY & FUTURE EXPERIMENTS	45
ACKNOWLEDGEMENTS	47
REFERENCES	49
PROGRAM ASSOCIATED PUBLICATIONS & PRESENTATIONS	51

PRECEDING PAGE BLANK NOT FILMED

ILLUSTRATIONS

<u>Figure</u>		<u>Page</u>
1	Co-Sm phase diagram for Co-rich region after Buschow et al (Ref. 19).....	3
2	Comparison of properties of MnBi (HC), Mn ₅₅ Al ₄₅ (τ), SmCo ₅ , Sm ₂ Co ₁₇ and Co compositions.....	4
3	Al-Mn phase diagram near Mn ₅₅ Al ₄₅ composition (a) and (b) relationship between disordered A3 (hexagonal), ordered B19 (orthorhombic) and metastable τ (tetragonal) phases after Van den Broek et al (Ref. 20)	5
4	Casting apparatus for Co-Sm and Al-Mn starting ingots.....	8
5	High temperature Bridgman-Stockbarger schematic ampoule of Co-Sm and Al-Mn alloys.....	9
6	Sample processing conditions for directional solidification of Co-Sm and Al-Mn alloys.....	11
7	Mellen Company, high temperature Bridgman-Stockbarger directional solidification facility.....	13
8	Temperature versus furnace position profiles for various solid materials in pyrolyzed, boron nitride (BN) ampoules for furnace hot and cold zone setting of 1500 and 1000 °C, respectively.....	14
9	Measured thermal gradient for selected thermal conductivity materials in high temperature directional solidification facility. For the thermal conductivities of liquid Co-Sm and Al-Mn alloys, a maximum gradient of approximately 60°C/cm is expected.....	15
10	As removed, directionally solidified Co-Sm alloys with starting compositions C ₀ = 12.0, 10.5 and 9.0 a/o Sm. Note brittle character of higher composition Sm alloys	18

ILLUSTRATION (CONTINUED)

<u>Figure</u>		<u>Page</u>
11	Optical micrograph montage of directionally solidified 9.0 a/o Sm, Co-Sm alloy solidified at a furnace velocity of $V = 10$ cm/h and G/V ratio of $\sim 2 \times 10^4$ °C-s/cm ²	19
12	Microstructure of directionally solidified 9 a/o Sm alloy processed at $V = 45.4$ cm/h in a thermal gradient of $G \sim 60$ °C/cm.....	20
13	Interdendrite eutectic structure transverse to solidification direction for Co-Sm alloy initially containing 9 a/o Sm and directionally solidified at $V = 45.4$ cm/h.....	21
14	(a) Classical morphological stability G/V criteria necessary for stable, cooperative growth (b) and solidification velocity (critical velocity) necessary for G/V criteria assuming $G_L = 60$ °C/cm versus Sm concentration in vicinity of $\text{Sm}_2\text{Co}_{17}/\text{Co}$ eutectic.....	23
15	Average composition of Sm in solid for initial composition $C_0 = 9.0$ a/o Sm directionally solidified at $V = 45.4$ cm/h. Curve is best x^2 -fit using Verhoeven model for off-eutectic, cooperative growth.....	24
16	Magnetization (at $H = 200$ kG) parallel to solidification direction as a function of sample length solidified. Superimposed are saturation magnetization values for $\text{Sm}_2\text{Co}_{17}$, theoretical value for 9 a/o Sm and Co. Sample's initial composition was 9 a/o Sm and was directionally solidified at $V = 45.4$ cm/h.....	25
17	Primary Co dendrite space (λ_D) and diameter (d_D), measured transverse of solidification direction, for near $\text{Sm}_2\text{Co}_{17}/\text{Co}$ eutectic composition (9 a/o Sm) as a function of inverse square root of furnace (solidification) velocity. Straight lines are least squares fit to higher velocity data.....	26

ILLUSTRATION (CONTINUED)

<u>Figure</u>		<u>Page</u>
18	Morphology transverse and longitudinal to solidification direction for initial composition $C_0 = 12.0$ a/o Sm ($\text{SmCo}_5/\text{Sm}_2\text{Co}_{17}$) directionally solidified at $V = 10$ cm/h.....	28
19	Magnetic domain pattern observed by Kerr effect in (a) ferro-magnetic SmCo_5 dendrites and (b) interdendritic $\text{SmCo}_5/\text{Sm}_2\text{Co}_{17}$ structure transverse to solidification direction for peritectic ($C_0 \sim 12.0$ a/o Sm) composition directionally solidified at $V = 10$ cm/h.....	29
20	Initial magnetization longitudinal (parallel) and transverse (perpendicular) to solidification direction for sample segment containing ~ 10.5 a/o Sm ($\sim \text{Sm}_2\text{Co}_{17}$). Observed anisotropy is consistent with easy axis of magnetization parallel to solidification direction.....	31
21	Magnetization per unit mass measured, at room temperature, parallel to solidification direction for near-eutectic (8.8 a/o Sm) and peritectic (12 a/o Sm) compositions.....	32
22	Selected region of directionally solidified Al-Mn alloy containing ~ 50 a/o Mn both transverse and longitudinal to solidification direction and grown at $V = 10$ cm/h.....	33
23	Measured (wet chemical analysis) bulk, longitudinal macro-segregation for Al-Mn sample containing initially ~ 55 a/o Mn and directionally solidified growth-up at $V = 10$ cm/h and $G \sim 55^\circ\text{C}/\text{cm}$	34
24	Initial magnetization measured parallel to the solidification direction as a function of fraction solidified (f) for sample displayed in Fig. 23.....	36
25	Magnetization in an applied magnetic field of 14 kOe measured parallel to the solidification direction versus Mn concentration for sample displayed in Figs. 23 and 24.....	37

ILLUSTRATIONS (CONTINUED)

<u>Figure</u>		<u>Page</u>
26	Ratio of magnetization measured parallel (long.) and perpendicular (trans.) to the solidification direction at an applied magnetic field of 14 kOe for fraction solidified ($f < 25\%$) regions containing τ -phase.....	38
27	Magnetization measured parallel to the solidification direction at 14 kOe versus fraction sample length solidified for samples initially containing ~55 a/o Mn and directionally solidified at $V = 10$ cm/h and 39.9 cm/h with $G \sim 55^\circ\text{C}/\text{cm}$	39
28	Selected region of directionally solidified Al-Mn alloy grown at $V = 10$ cm/h and heat treated 1h at 800°C in argon atmosphere. Sample segment composition is ~50 a/o Mn.....	41
29	Demagnetization behavior of directionally solidified Al-Mn alloy segment containing ~50 a/o Mn measured parallel to the solidification direction in as-grown and post heat-treated states.....	42
30	Initial magnetization and hysteresis curve for heat treated Al-Mn segment containing ~50 a/o Mn and measured parallel to solidification direction.....	43

ABSTRACT

This report summarizes the final year effort whose goal was to determine the effects of directional solidification processing on the microstructural, compositional and magnetic properties of high-melting-temperature, commercially important alloys which form from the liquid state via peritectic or eutectic type reactions. The final year's effort was preliminary in scope and was intended to utilize insight gained during the first two years, which dealt primarily with the model system Bi-Pb. During the final year, emphasis was placed on ferromagnetic compounds of the commercially important Co-Sm and Al-Mn systems. In particular, bulk compositions corresponding to peritectic $\text{SmCo}_5/\text{Sm}_2\text{Co}_{17}$ (12 a/o Sm), $\text{Sm}_2\text{Co}_{17}$ (10.5 a/o Sm), eutectic $\text{Sm}_2\text{Co}_{17}/\text{Co}$ (9 a/o Sm) and peritectic $\text{Mn}_{55}\text{Al}_{45}$ (55 a/o Mn) were studied.

Because these systems have high melting temperatures ($T_m > 1000^\circ\text{C}$) and are quite reactive to oxidizing environments, special containment techniques during solidification were developed. These techniques included use of pyrolytic boron nitride ampoules that were pumped to a vacuum of 10^{-6} torr prior to directional solidification. The ampoule arrangement was housed within a specially constructed, high temperature Bridgman-Stockbarger directional solidification furnace consisting of three actively controlled heating/cooling zones.

Initial investigations have been performed at modest thermal gradients in the liquid, $G_L < 60^\circ\text{C}/\text{cm}$, and over a range of furnace (solidification) velocities, $0.8 < V < 45.4 \text{ cm/h}$. Since the range of G_L/V values, a measure of the degree of interfacial morphological stability, was rather low, i.e., $.05 < G_L/V < 2.7 \times 10^5 \text{ }^\circ\text{C}\cdot\text{s}/\text{cm}^2$, aligned dendritic morphologies were encountered for the Co-Sm system. The primary dendrite spacing for eutectic $\text{Sm}_2\text{Co}_{17}/\text{Co}$ scaled with $V^{1/2}$ and varied from $\sim 50 \text{ }\mu\text{m}$ for $V > 20 \text{ cm/h}$ to hundreds of microns for $V < 10 \text{ cm/h}$. Since the crystal growth mechanism was dendritic rather than cooperative, the associated permanent magnet properties were rather poor, e.g., remanence less than 3 kG and coercive force less than 1 kOe for the smallest dendrite sizes encountered. Magnetization as a function of sample orientation indicated that the easy axis of magnetization was primarily along the direction of solidification for the eutectic $\text{Sm}_2\text{Co}_{17}/\text{Co}$ and peritectic $\text{SmCo}_5/\text{Sm}_2\text{Co}_{17}$ compositions.

the direction of solidification for the eutectic $\text{Sm}_2\text{Co}_{17}/\text{Co}$ and peritectic $\text{SmCo}_5/\text{Sm}_2\text{Co}_{17}$ compositions.

For the Al-Mn case, magnetization and microstructural characterization suggested isotropic, polycrystalline growth for all solidification velocities studied, with appreciable macrosegregation observed in the lower growth velocity range ($V < 10 \text{ cm/h}$) . For the composition of interest, i.e. 55 at/o Mn, appreciable ferrimagnetic $\tau\text{-MnAl}$ phase was found to form at the higher solidification velocities (higher cooler rates) in agreement with previous studies. Subsequent annealing, after solidification, was found to enhance magnetic performance.

INTRODUCTION

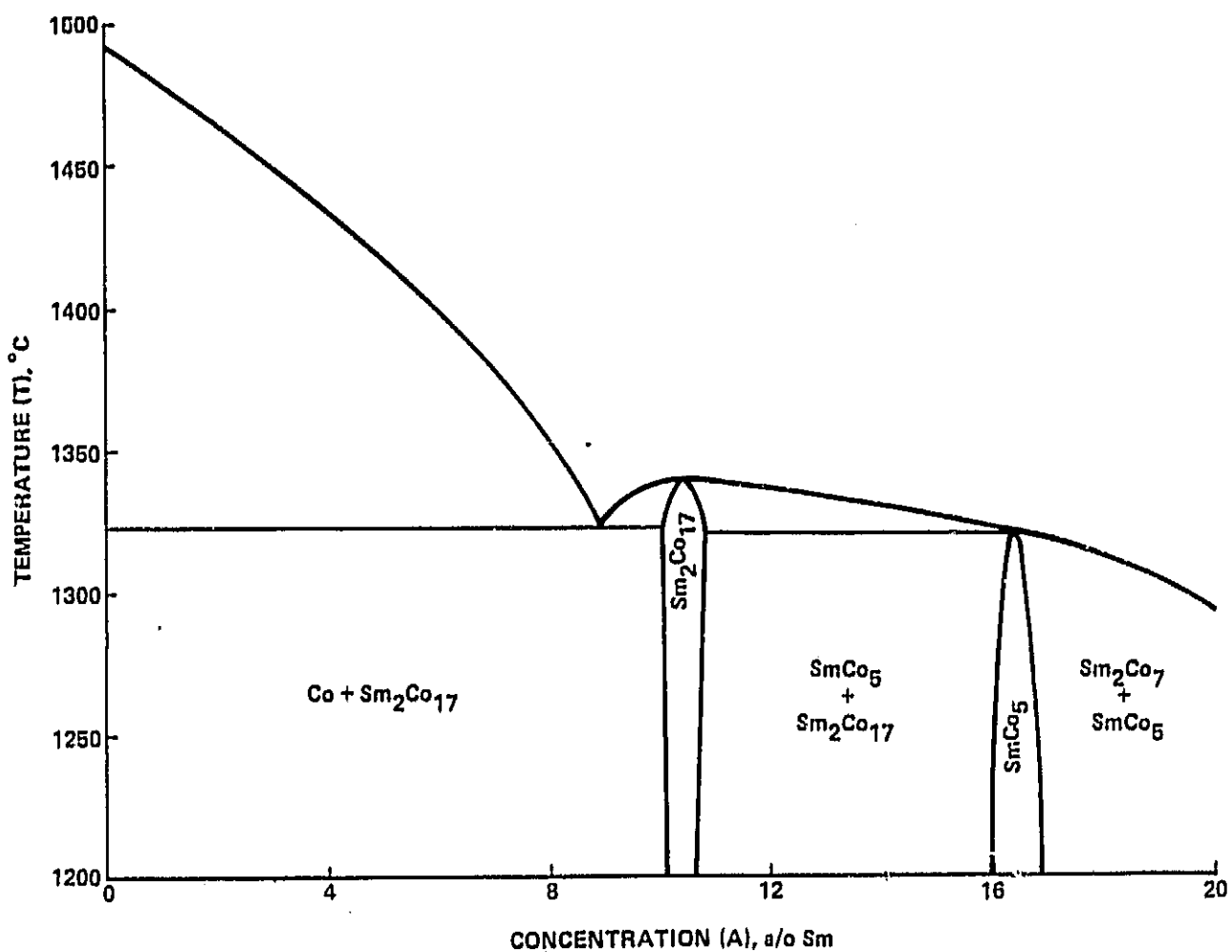
Extensive effort has been carried out over the last several years involving rare-earth/transition metal (Refs. 1-3) and transition/normal metal (Ref. 4) based alloys. The primary objective to these studies has been to produce new permanent magnets exhibiting improved magnetic properties. This effort has led to commercial production of permanent magnets with energy products on the order of 20 MG-Oe (Ref. 5), i.e. about 60% of the theoretical maximum for this class of materials (Ref. 6). The fabrication of these materials, with stable and reproducible magnetic properties which approach the theoretical maximum, has proven difficult (Ref. 7) because of current processing technique limitations. Directional solidification processing has been shown to produce composite morphologies, for low volume fraction, ferromagnetic eutectic and off-eutectic forming alloys, which exhibit aligned fibrous and crystallographic characteristics advantageous for enhanced magnetic performance (Refs. 8-9).

The scope of the present effort was twofold: First, to investigate the applicability of directional solidification of high melting temperature, commercially relevant compounds to produce aligned fibrous and lamellar morphologies and quantify their magnetic performance. Selected compositions which form via eutectic or off-eutectic liquid-solid reactions were chosen from the commercially important Co-Sm system. The Co-Sm system was investigated because certain of its phases possess theoretically, as shown in Figs. 1 and 2, the largest permanent magnetic figures of merit (Ref. 6), form via eutectic or off-eutectic reactions and because of our previous experience with magnetic property characterization of compounds from this system (Ref. 10). A second thrust was to determine whether coupled, cooperative growth of phases from the Co-Sm and Al-Mn system, which solidify via a peritectic reaction (Figs. 1 and 3), occurred using the Bridgman-Stockbarger directional solidification method. The Al-Mn system was investigated because one of its phases the so-called τ -phase of $Mn_{55}Al_{45}$ stoichiometry, originally solidified via a peritectic reaction as shown in Fig. 3. Also, its magnetic properties are similar to those of the non-equilibrium HC MnBi phase, Fig. 2, which we

have extensively characterized in studies of directionally solidified Bi-Mn alloys (Refs. 11-12). In addition, the density of Al near the solidification temperature of $Mn_{55}Al_{45}$ ($\sim 1240^{\circ}C$) is only 50% that of Mn so that appreciable solutal convection is anticipated. This is in contrast to the Co-Sm system, in which the densities of liquid Sm and Co are nearly equal at the solidification temperatures of the peritectic forming phases studied, i.e. $SmCo_5$ ($\sim 1320^{\circ}C$) and Sm_2Co_{17} ($\sim 1340^{\circ}C$).

The Bridgman-Stockbarger approach is an attractive candidate for processing peritectic forming compounds. However, the theoretically anticipated and electronically advantageous aligned fibrous or lamellar microstructures have never been experimentally observed (Refs. 13-14). If these microstructures could be produced, benefits not only to permanent magnet performance but also to magnetoelastic, magneto-optical and superconducting materials could result since many materials with these important properties solidify via a peritectic reaction.

It should be noted that this investigation was preliminary in scope and hence focused on a qualitative evaluation. As a result of these efforts, future one and low-gravity studies will be conducted as part of our long term "Orbital Processing of Aligned Magnetic Composites" contract (NAS8-32948).

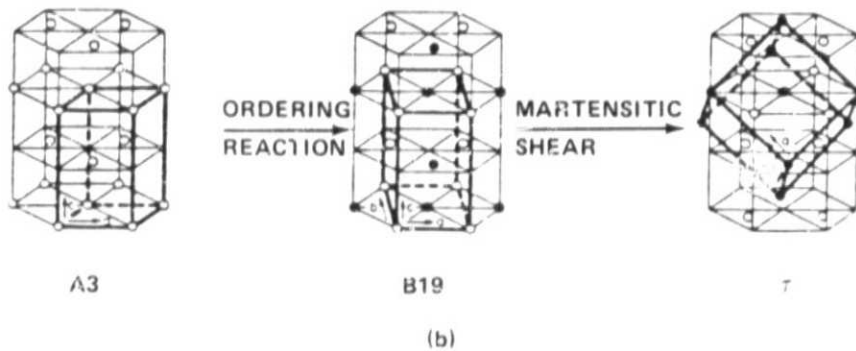
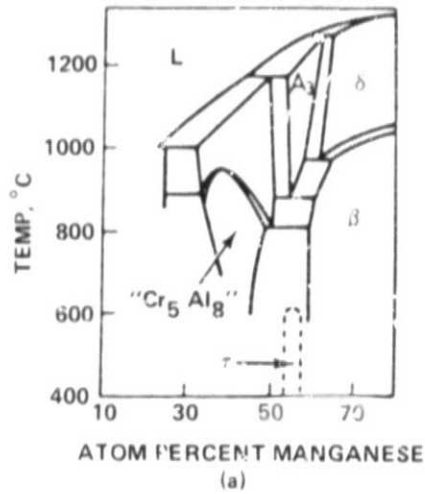


R84-1309-001(T)

Fig. 1 Co-Sm phase diagram for Co-rich region after Buschow et al (Ref. 19)

PROPERTY	COMPOUND	MnBi (HC)	Mn55Al45 (r)	SmCo5	Sm2Co17	Co
CRYSTAL STRUCTURE		ORTHORHOMBIC	TETRAGONAL (CuAu II)	HEXAGONAL (CaCu5)	HEXAGONAL (Th2Ni17)	HEXAGONAL
TYPE OF MAGNETIC ORDERING		FERRI	FERRI	FERRI	FERRI	FERRI
EASY AXIS OF MAGNETIZATION		C-AXIS	C-AXIS	C-AXIS	C-AXIS	C-AXIS
DENSITY, g/cm ³		9.0	5.1	8.60	8.57	8.80
CRYSTAL ANISOTROPY CONSTANT (K ₁), erg/cc x 10 ⁶ AT ROOM TEMP		12	11	171	20	4.1
NUCLEATION OR CRYSTAL FIELD (H _N), Oe x 10 ³		120	30	400	65-95	6.0
SPONTANEOUS MAGNETIZATION (M _s), GAUSS AT ROOM TEMP		220	350	850	955	1400
CRITICAL DIAMETER FOR SINGLE DOMAIN BEHAVIOR (D _c), μm		0.5	0.3	1.1	0.5	0.08
CURIE TEMPERATURE, °C		-33	320	693	934	1127
1309-002(T)						

Fig. 2 Comparison of properties of MnBi (HC), Mn55Al45(r), SmCo5, Sm2Co17 and Co compositions



R84-1309-003(T)

Fig. 3 Al-Mn phase diagram near Mn₅₅Al₄₅ composition (a) and (b) relationship between disordered A3 (hexagonal), ordered B19 (orthorhombic) and metastable τ (tetragonal) phases after van den Brock et al (Ref. 20)

have extensively characterized in studies of directionally solidified Bi-Mn alloys (Refs. 11-12). In addition, the density of Al near the solidification temperature of $Mn_{55}Al_{45}$ ($\sim 1240^{\circ}C$) is only 50% that of Mn so that appreciable solutal convection is anticipated. This is in contrast to the Co-Sm system, in which the densities of liquid Sm and Co are nearly equal at the solidification temperatures of the peritectic forming phases studied, i.e. $SmCo_5$ ($\sim 1320^{\circ}C$) and Sm_2Co_{17} ($\sim 1340^{\circ}C$).

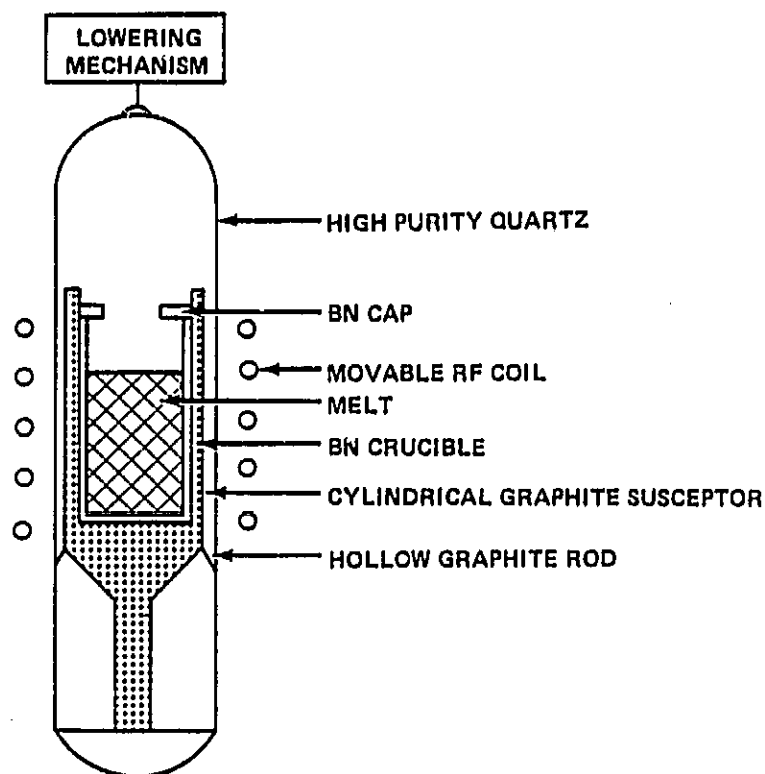
The Bridgman-Stockbarger approach is an attractive candidate for processing peritectic forming compounds. However, the theoretically anticipated and electronically advantageous aligned fibrous or lamellar microstructures have never been experimentally observed (Refs. 13-14). If these microstructures could be produced, benefits not only to permanent magnet performance but also to magnetoelastic, magnetooptical and superconducting materials could result since many materials with these important properties solidify via a peritectic reaction.

It should be noted that this investigation was preliminary in scope and hence focused on a qualitative evaluation. As a result of these efforts, future one and low-gravity studies will be conducted as part of our long term "Orbital Processing of Aligned Magnetic Composites" contract (NAS8-32948).

EXPERIMENTAL PROCEDURES

Sample Preparation

Starting material was prepared from commercially pure Al (99.999 weight percent (w/o)), Co (99.999 w/o), Mn (99.9 w/o) and Sm (99.9 w/o) powder (325-mesh) obtained from the Alfa Division of the Ventron Corporation. Specific alloy compositions corresponding to ~25 volume percent (v/o) SmCo_5 and ~75 v/o $\text{Sm}_2\text{Co}_{17}$ (12 atomic percent (a/o) Sm), $\text{Sm}_2\text{Co}_{17}$ (10.5 a/o Sm), eutectic $\text{Sm}_2\text{Co}_{17}/\text{Co}$ (9 a/o Sm) and peritectic $\text{Mn}_{55}\text{Al}_{45}$ (55 a/o Mn) were fabricated by first mechanically mixing the selected powder proportions, placing in open pyrolyzed boron nitride (BN) crucibles and heat treating below their melting points in a vacuum ($<10^{-6}$ torr) furnace for 2 h. Pyrolyzed BN was chosen after previous studies to evaluate crucible materials capable of containing molten Co-Sm alloys (Ref. 15). The outgassed mixtures were then encapsulated in pyrolyzed BN cylindrical ampoules (0.7 cm inner diameter by 10.0 cm in length) open at one end, which were sealed within a quartz ampoule ($<10^{-6}$ torr), as shown in Fig. 4. The entire ampoule arrangement was suspended in a RF induction heater and electromagnetically melted and stirred (450 Hz frequency and 10 kW power) for 2 h to insure homogenization. Care was taken to slowly raise the temperature of the powder until melting occurred as observed optically by means of an IR pyrometer. The temperature was then maintained a few degrees above each composition's melting point during homogenization in order to minimize vapor transport of volatile phases. A rapid cooling (\sim few $^{\circ}\text{C}/\text{s}$) was achieved by abruptly shutting off the induction unit after sample melting and homogenization. Homogeneity was checked on selected samples by wet chemical analysis, and variance in composition was found to be less than 0.2 w/o Sm (for Co-Sm alloys) and 0.1 w/o Mn (for Al-Mn alloys) over the length of 7.5 cm samples. Each of these samples was removed from their BN ampoules and the outer surface skin, presumably a SmN or MnN reaction product localized to a thin film at the melt-crucible interface, was removed abrasively. Each sample was then encapsulated in a sealed, pyrolyzed BN ampoule which was placed on a graphite pedestal (heatsink) and housed in an evacuated Al_2O_3 outer tube as shown in Fig. 5. The ampoule arrangement was



R84-1309-004(T)

Fig. 4 Casting apparatus for Co-Sm and Al-Mn starting ingots

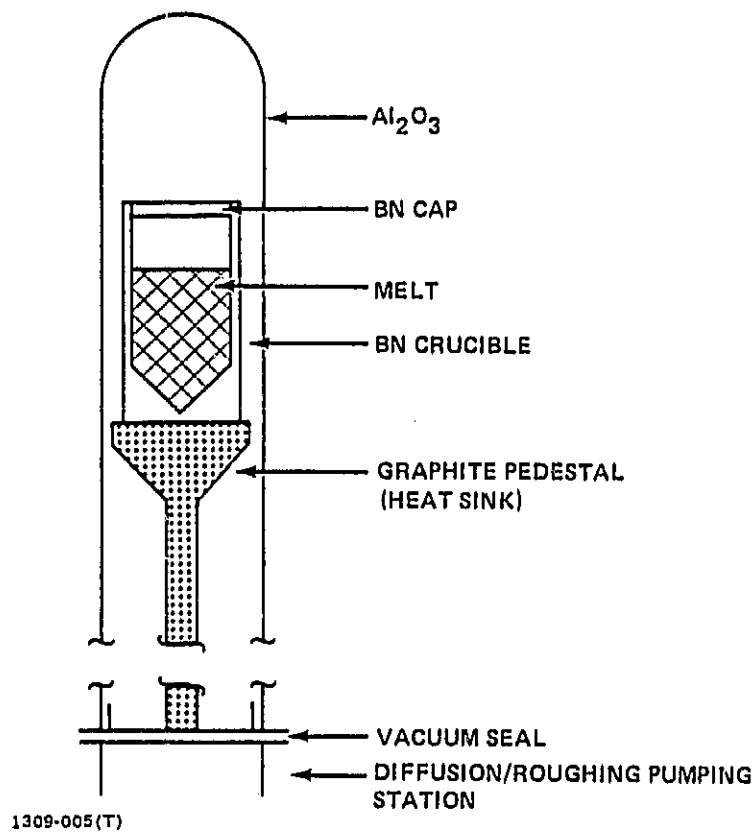


Fig. 5 High temperature Bridgman-Stockbarger schematic ampoule for directional solidification

actively pumped ($<10^{-5}$ torr) at temperature below the specific sample's melting point for 1h and then sealed prior to directional solidification.

Experiment Composition/Test Matrix

A series of alloy compositions corresponding to $\text{SmCo}_5/\text{Sm}_2\text{Co}_{17}$ (12 a/o Sm), $\text{Sm}_2\text{Co}_{17}$ (10.5 a/o Sm), eutectic $\text{Sm}_2\text{Co}_{17}/\text{Co}$ (9.0 a/o Sm) and $\text{Mn}_{55}\text{Al}_{45}$ (55 a/o Mn) were selected for this preliminary study because they span the types of solidification which occur for the commercially important alloys in these systems. Growth velocities and hot/cold zone temperatures were chosen to produce the optimum G_L/V ratios, minimum microstructural phase dimensions (optimum magnetic performance) and yet maintain the location of the liquid-solid interface within the furnace's adiabatic zone (directional heat flow). Since this study was preliminary in scope, all solidification was performed in a growth-up (antiparallel to the gravity direction) orientation which should minimize thermal convection. A list of growth conditions and alloy compositions studied is shown in Fig. 6.

Directional Solidification Processing

This final year's effort was intended to utilize insight gain during the initial two years of this program, which dealt with the Bi-Pb system. However, since the phases of the Bi-Pb system are non-ferromagnetic, can be routinely contained and processed in standard quartz ampoules and have rather low melting temperatures ($T_m < 327^\circ\text{C}$), the analogy to directional solidification of the Co-Sm and Al-Mn systems was limited to insight relating to heat transfer and positioning of the solidification interface within the adiabatic furnace zone during solidification. During the first two years of this program, it was determined that the position of the solidification interface was strongly dependent on the temperature difference between the furnace hot and cold zones and furnace velocity (Ref. 16). If these solidification parameters are not appropriately selected, the position of the solidification interface could lie within either the hot or cold zones of the furnace thus leading to appreciable interface curvature, radial thermal gradients and morphological instabilities. In fact, for the Bi-Pb system,

ALLOY COMPOSITION	COMPOUND(S)	HOT ZONE TEMP, °C	COLD ZONE TEMP, °C	FURNACE VELOCITY (V), cm/h	THERMAL GRADIENT (G _L), °C/cm	G _L /V, °C · s/cm ²
9.0 a/o Sm 91.0 a/o Co	EUTECTIC Sm ₂ Co ₁₇ /Co	1500	1000	2.7	~ 60	8.0 × 10 ⁴
		1500	1000	10.0	~ 60	2.2 × 10 ⁴
		1500	1000	20.0	~ 60	1.1 × 10 ⁴
		1500	900	45.4	~ 60	4.8 × 10 ³
10.5 a/o Sm 89.5 a/o Co	Sm ₂ Co ₁₇	1500	1000	2.7	~ 60	8.0 × 10 ⁴
		1500	1000	10.0	~ 60	2.2 × 10 ⁴
		1500	900	35.9	~ 60	6.0 × 10 ³
12.0 a/o Sm 88.0 a/o Co	PERITECTIC SmCo ₅ /Sm ₂ Co ₁₇	1500	1000	2.5	~ 60	8.6 × 10 ⁴
		1500	1000	10.0	~ 60	2.2 × 10 ⁴
55.0 a/o Mn 45.0 a/o Al	PERITECTIC Mn ₅₅ Al ₄₅	1500	1000	0.8	~ 55	2.5 × 10 ⁵
		1500	1000	10.0	~ 55	2.0 × 10 ⁴
		1500	900	39.9	~ 55	5.0 × 10 ³
1309-006(T)						

Fig. 6 Sample processing conditions for directional solidification of Co-Sm and Al-Mn alloys

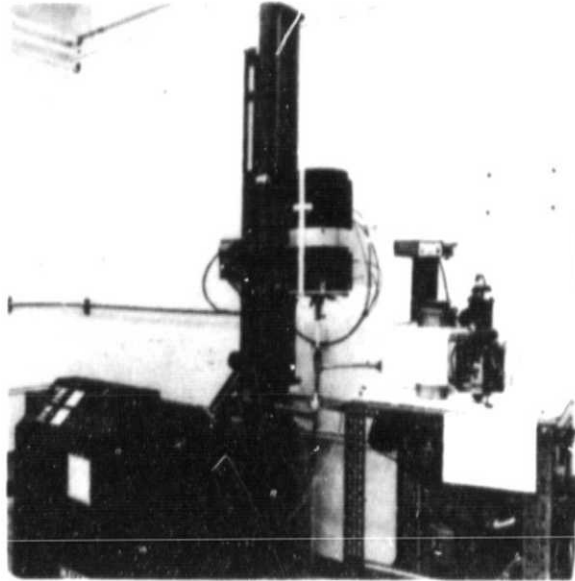
microstructural banding and lack of thermal control (non-unidirectional heat flow at the solidification interface) was found to occur if the furnace hot zone/cold zone temperature difference was too large even for low furnace velocities (Ref. 15). Therefore, care was taken to select the furnace hot and cold zone temperatures so as to maintain a linear solidification interface at a chosen furnace velocity, as shown in Fig. 6,

Directional solidification was performed using the Bridgman-Stockbarger method in a high temperature apparatus purchased from the Mellen Company. This apparatus consists of a three zone Bridgman-Stockbarger type furnace assembly capable of translating at velocities V , $0.8 < V < 50$ cm/h, and hot zone temperatures up to 1600°C . This assembly is shown in Fig. 7. The furnace assembly/ampoule arrangement was thermally characterized using Pt-Rh thermocouples incorporated into solids, within pyrolyzed BN ampoules, of various thermal conductivities. The thermal characteristics of an unloaded, unevacuated (air) BN ampoule was also measured. As shown in Figs. 8 and 9, the attainable thermal gradient that could be maintained between 1100 and 1300°C , i.e., the range of solidification temperatures anticipated for the Co-Sm and Al-Mn compositions of interest, varied from $\sim 80^{\circ}\text{C}/\text{cm}$ for high conductivity conditions to $\sim 50^{\circ}\text{C}/\text{cm}$ for low conductivity materials. These conditions were achieved for a hot zone furnace temperature of 1500°C and cold zone temperature of 900 and 1000°C with $1100 < T < 1300^{\circ}\text{C}$ occurring within the adiabatic zone. Also shown in Fig. 9 are the anticipated thermal conductivities for liquid Co-Sm and Al-Mn compositions of interest. Therefore, the range of achievable G_L/V (thermal gradient in liquid at the liquid-solid interface, $G_L/\text{furnace (solidification) velocity, } V$) was deduced to vary from $G_L/V \sim 5 \times 10^3 \text{ }^{\circ}\text{C}\cdot\text{s}/\text{cm}^2$ at $V = 50 \text{ cm/h}$ to $G_L/V \sim 2.5 \times 10^5 \text{ }^{\circ}\text{C}\cdot\text{s}/\text{cm}^2$ at $V = 0.8 \text{ cm/h}$.

Microstructural & Microchemical Characterization

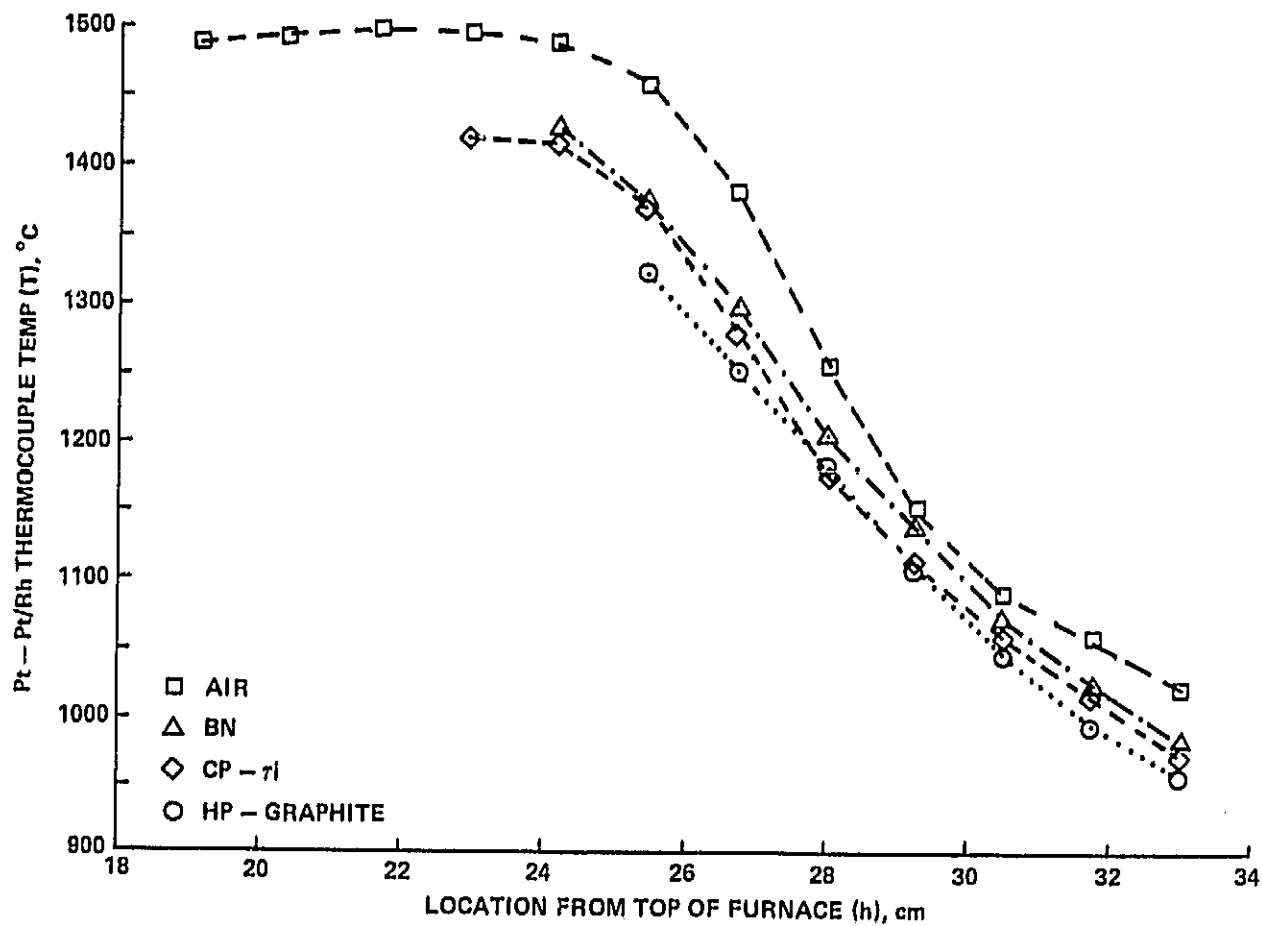
Directionally solidified samples were prepared for metallographic examination using standard abrasive polishing techniques. After polishing, a dilute HCl acid etch was applied to enhance phase contrast. Micrographs both transverse and longitudinal to the solidification direction were obtained

ORIGINAL
OF POOR QUALITY



R84-1309-007(T)

Fig. 7 Mellen Company, high temperature Bridgman-Stockbarger directional solidification facility



R84-1309-008(T)

Fig. 8 Temperature versus furnace position profiles for various solid materials in pyrolyzed, boron nitride (BN) ampoules for a furnace hot and cold zone setting of 1500 and 1000°C, respectively.

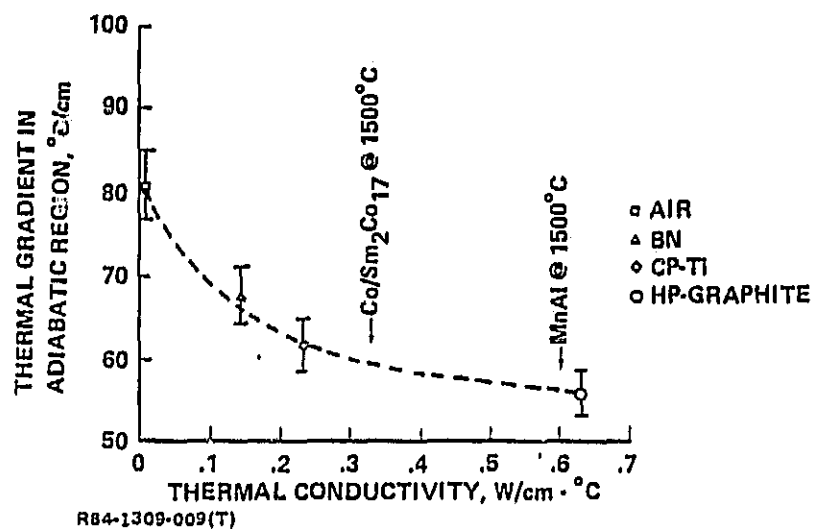


Fig. 9 Measured thermal gradients for selected thermal conductivity materials in high temperature directional solidification facility. For the thermal conductivities of liquid Co-Sm and Al-Mn alloys, a maximum gradient of approximately $60^{\circ}\text{C}/\text{cm}$ is expected

using conventional optical microscopy. Selected eutectic $\text{Sm}_2\text{Co}_{17}/\text{Co}$ alloys were analyzed for primary Co dendrite spacing in the $\text{Sm}_2\text{Co}_{17}$ matrix using a Leitz particle size analysis technique developed for directionally solidified Bi-Mn (Ref. 7).

Selected microscopic regions (~ hundreds of microns in size) were analyzed by energy dispersive x-ray analysis on an AMR-1000 scanning electron microscope to determine composition of various phases.

In addition, Kerr magneto-optical microscopy, which utilizes the preferential magnetic scattering of incident plane polarized light by the magnetic domains (Ref. 19) was used to observe the magnetic domain structure. It is at phase interfaces (inhomogeneous magnetic surfaces) that reverse domains are thought to nucleate and therefore limit the potentially large nucleation fields (Fig. 2) for this class of materials (Ref. 6).

Magnetic Property Characterization

Magnetization of cylindrically shaped samples was measured parallel to the solidification direction at 290 K (room temperature) and 77 K in applied fields up to 200 kG using a low frequency vibrating sample magnetometer at the Francis Bitter National Magnet Laboratory. A Princeton Applied Research high frequency vibrating sample magnetometer was used to measure room temperature magnetization as a function of angle with respect to solidification direction and applied fields up to 15 kOe at Grumman's R&D Center.

RESULTS & DISCUSSION

General Observations

The morphology of directionally solidified Co-Sm samples, with starting compositions of 9, 10.5 and 12.0 a/o Sm, exhibited qualitatively, uncoupled dendrite structures. The overall mechanical consistency for this range of compositions was much better for the lower Sm composition alloys, as shown in Fig. 10. The amount of porosity and brittleness was rather low for 9 a/o Sm and was found to increase with increasing Sm content.

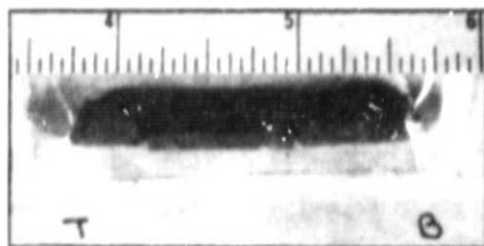
The morphology of directionally solidified Al-Mn samples, with starting compositions ~55 a/o Mn, consisted of randomly oriented fibers dispersed in a textureless phase for the composition region of interest, i.e. 40 - 55 a/o Mn. Other Al-Mn phases occurred, due to macrosegregation, such as $MnAl_4$ and $MnAl_5$, but were found in the latter regions to solidify and were not analyzed. The mechanical consistency, for compositions between 40 and 55 a/o Mn, was good with no appreciable cracking or porosity observed after directional solidification processing

Sm_2Co_{17} /Co Eutectic

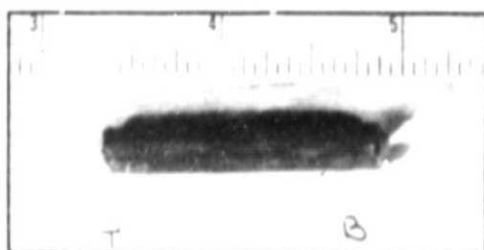
The microstructure of directionally solidified, 9 a/o Sm alloy samples contained primary, aligned Co dendrites within an aligned Sm_2Co_{17} matrix as seen in Fig. 11. The degree of crystallographic alignment was inferred from magnetization measurements performed parallel and perpendicular to the solidification direction. For all processing conditions (Fig. 6), the c-axis (easy axis of magnetization) of both the hexagonal Co and Sm_2Co_{17} phases were approximately along the solidification (heat transfer) direction.

A closer examination of the microstructure, Fig. 12, revealed another phase, presumably the true Sm_2Co_{17} /Co eutectic, surrounding the primary Co dendrites. A higher magnification photomicrograph, Fig. 13, is suggestive of a lamellar-like structure. This suggests that coupled eutectic growth may be possible in this system if the melt composition is sufficiently close to the true eutectic composition and if a sufficiently large thermal gradient in the

ORIGINAL PAGE IS
OF POOR QUALITY



$C_0 = 12.0$ a/o Sm



$C_0 = 10.5$ a/o Sm

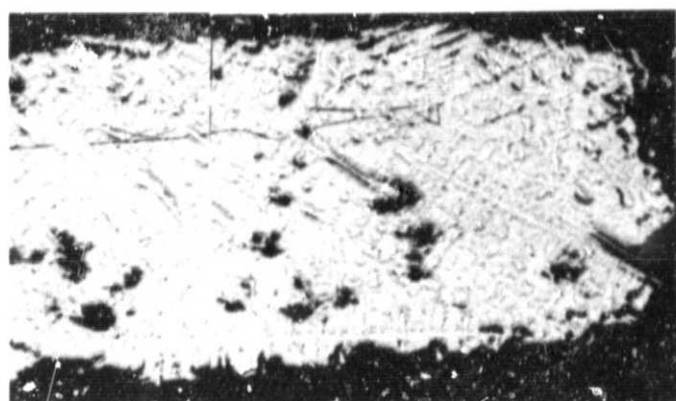
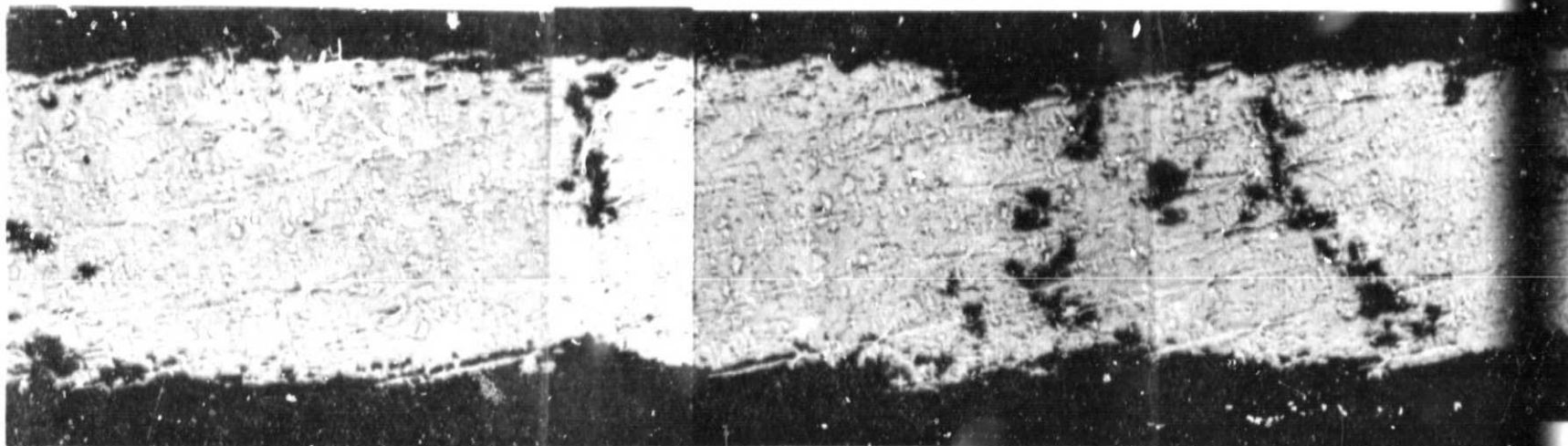
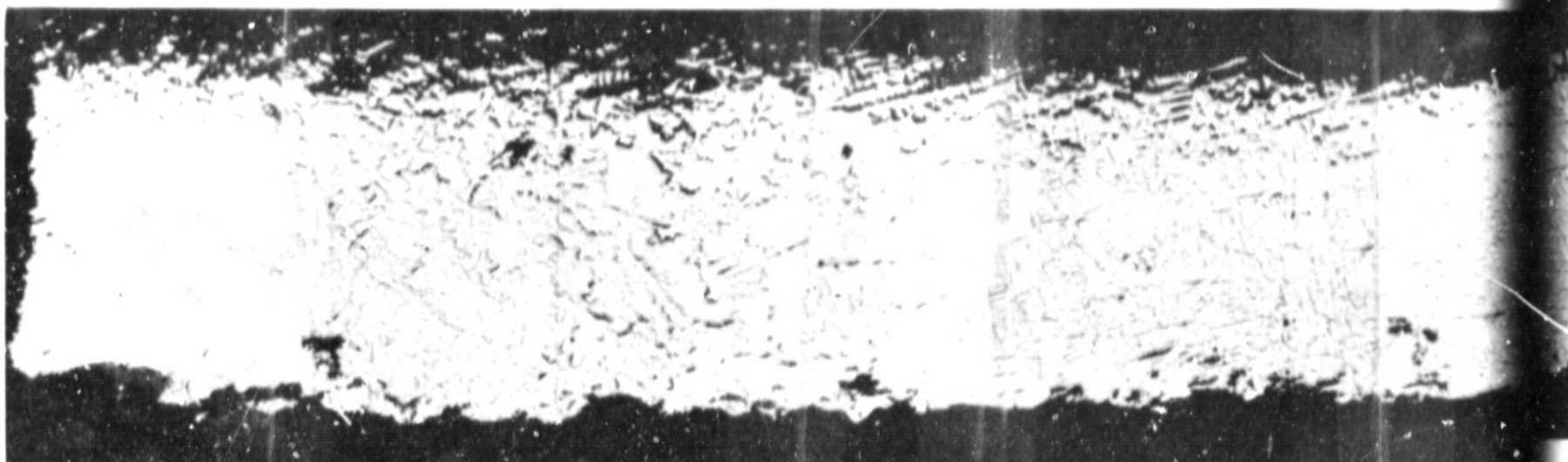


$C_0 = 9.0$ a/o Sm

R84-1309-010(T)

Fig. 10 As removed, directionally solidified Co-Sm alloys with starting compositions $C_0 = 12.0$, 10.5 and 9.0 a/o Sm. Note brittle character of higher composition Sm alloys

PRODUCT NAME

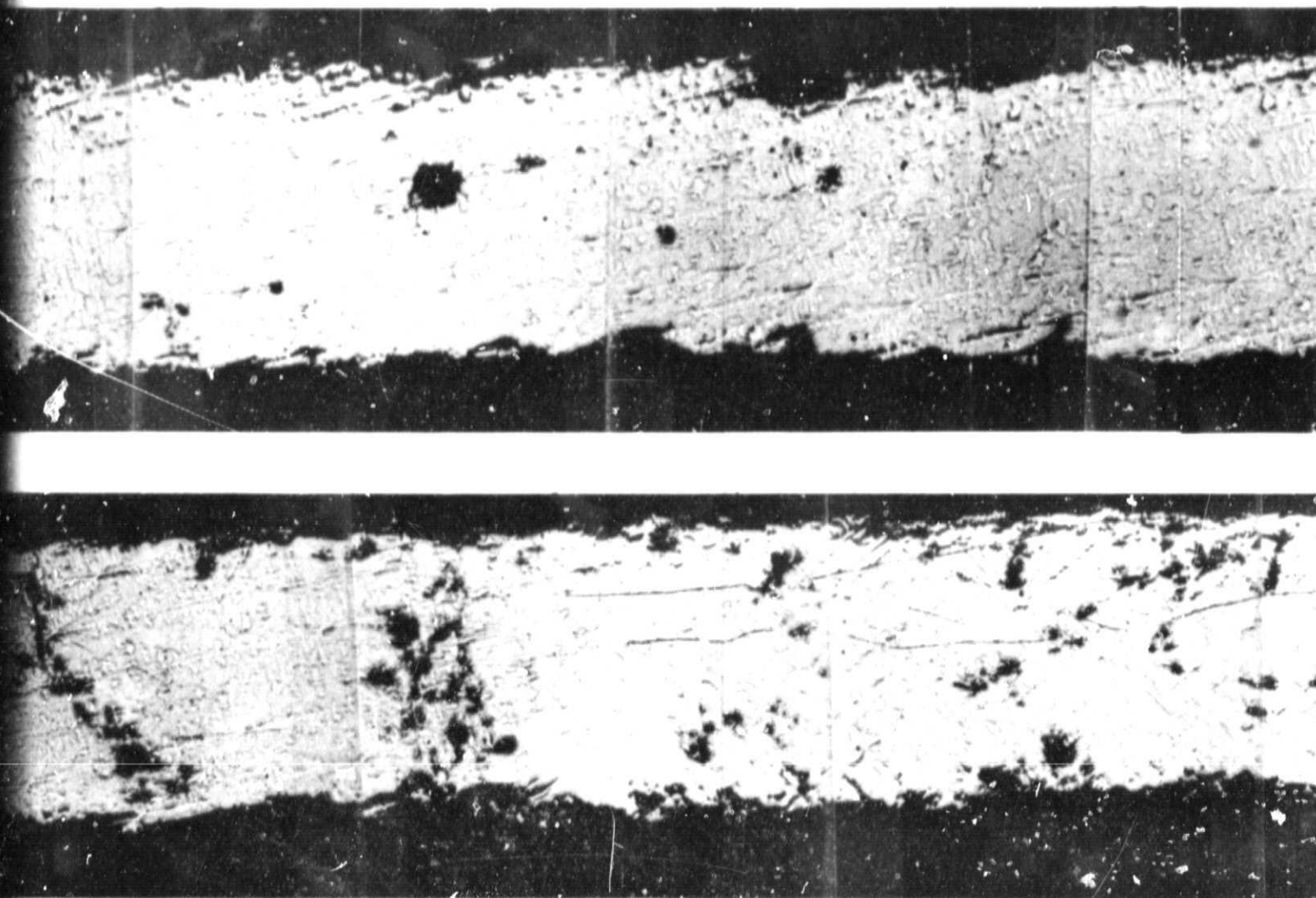


5 mm

GROWTH
DIRECTION

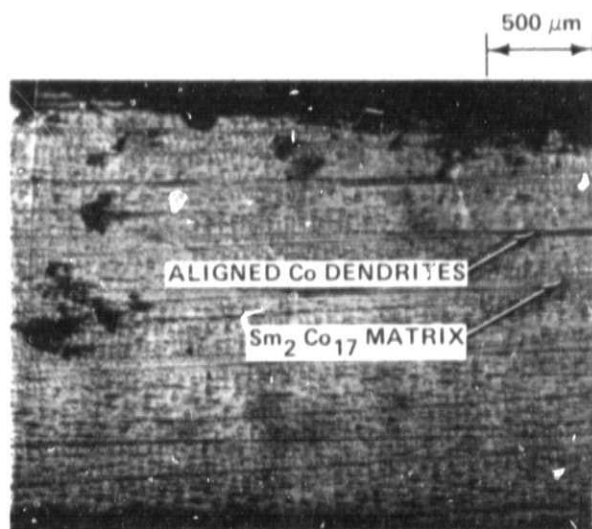
R84-1309 011(T)

OF POOR QUALITY

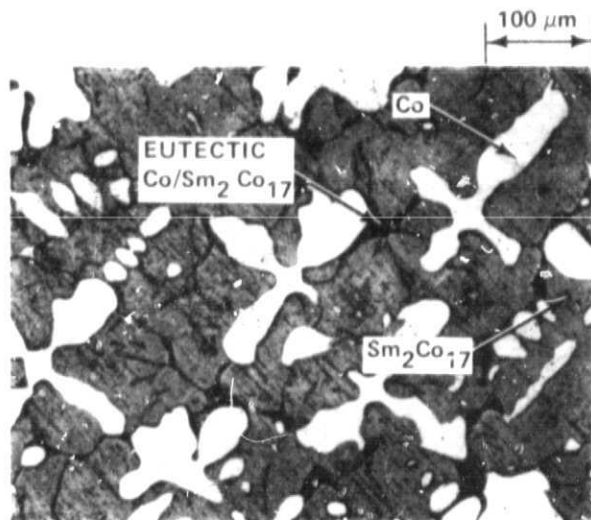


5 mm

Fig. 11 Optical micrograph montage of directionally solidified 9.0 a/o Sm, Co-Sm alloy solidified at a furnace velocity of $V = 10 \text{ cm/h}$ and G/V ratio of $\sim 2 \times 10^4 \text{ }^\circ\text{C-s/cm}^2$.



a. Longitudinal to Growth Direction-Note
Aligned Dendritic Structure



b. Dendritic Structure Transverse Growth Direction

R84-1309-012(T)

Fig. 12 Microstructure of directionally solidified 9 a/o
Sm alloy processed at $V = 45.4 \text{ cm/h}$ in a thermal
gradient of $G \sim 60^\circ\text{C/cm}$

ORIGINAL FILED
OF POOR QUALITY

ORIGINAL
OF POOR QUALITY

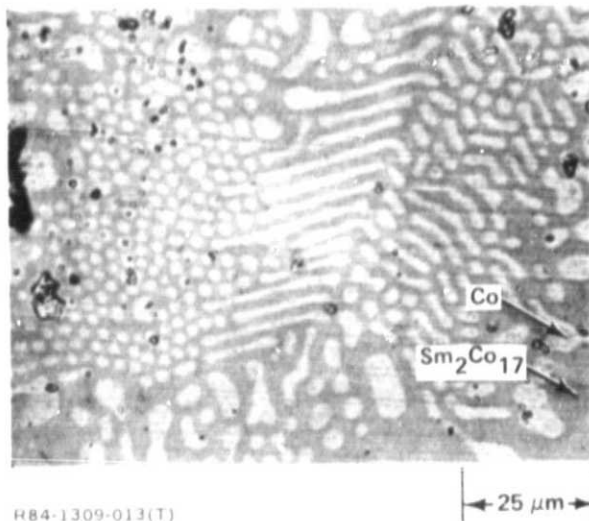
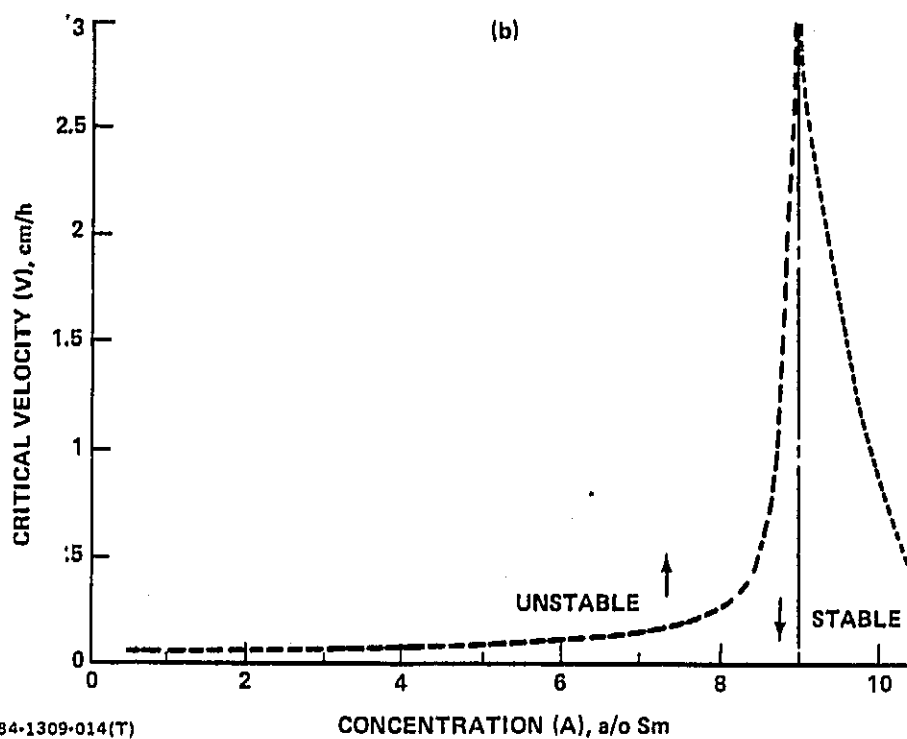
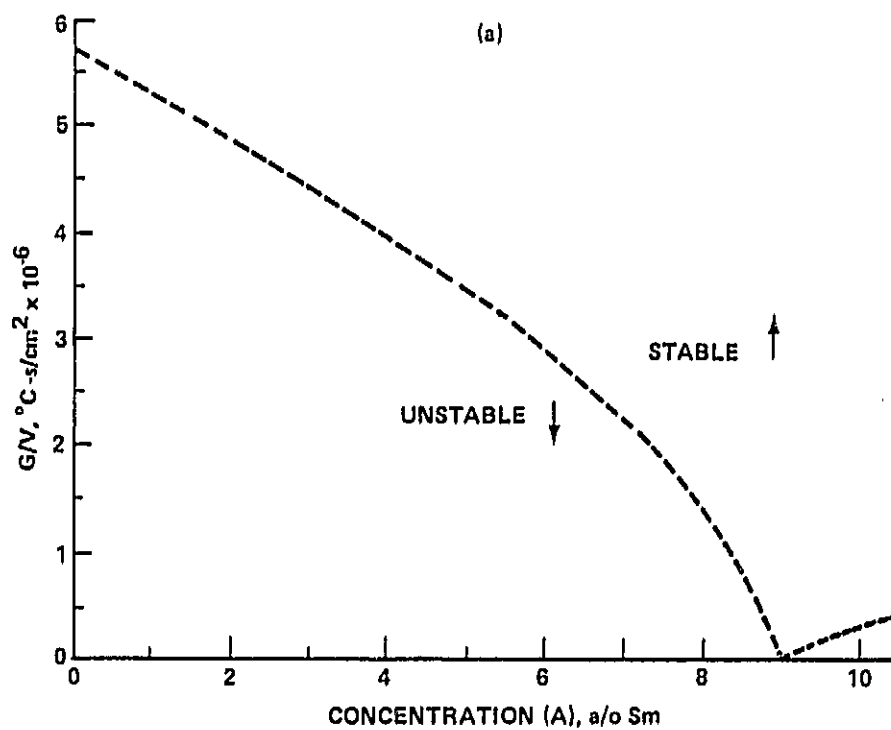


Fig. 13 Interdentrite eutectic structure transverse to solidification direction for Co-Sm alloy initially containing 9 a/o Sm and directionally solidified at $V = 45.4 \text{ cm/h}$

liquid near the liquid-solid interface is established so that the interface is maintained essentially isothermal. An examination of the classical G/V , morphological stability criteria for this system (Fig. 14a) and the solidification velocity (critical velocity) necessary to maintain cooperative, coupled growth (Fig. 14b) at the estimated, available liquid thermal gradient of $G \sim 60$ °C/cm, shows the near-eutectic stoichiometry must be attained (<0.1 a/o Sm) in order to achieve coupled, cooperative growth even at the lowest solidification velocity used, i.e. $V = 2.7$ cm/h (see Fig. 6).

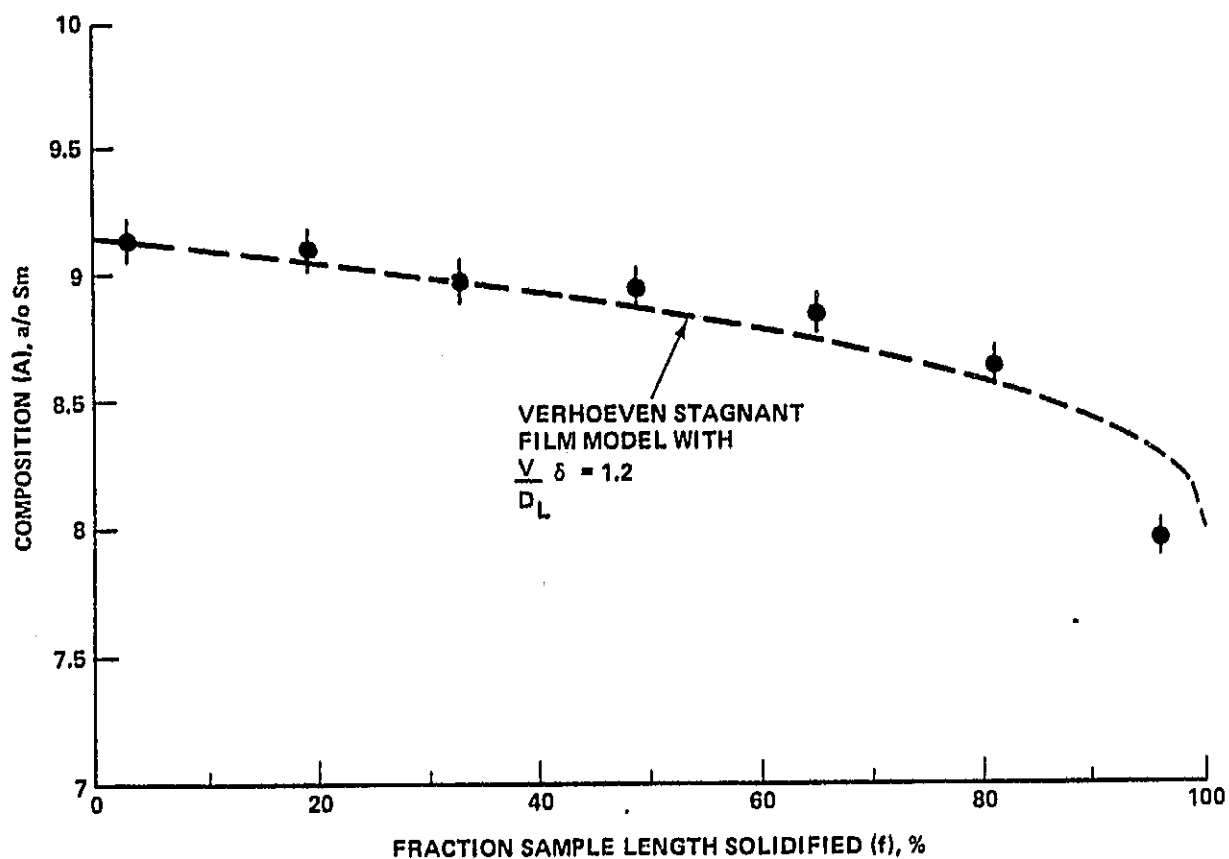
Surprisingly, appreciable macrosegregation was observed even at the highest solidification velocities studied. Qualitatively, the degree of macrosegregation increased linearly with decreasing solidification velocity. As shown in Fig. 15, the Sm composition was found to vary from ~ 9.2 a/o Sm during the initial phase of solidification to ~ 8.0 a/o Sm near the end of solidification for a sample containing 9 a/o Sm and directionally solidified at $V = 45.4$ cm/h. Also shown are a best fit to the observed composition segregation using an off-eutectic solidification model developed by Verhoeven et al (Ref. 21), where D_L is the liquid diffusivity (assumed to be $\sim 10^{-5}$ cm²/s) and δ is the characteristic, stagnant film thickness inside of which mass and heat transfer are controlled only by diffusion. Even though this model assumes coupled growth, the dendritic growth data appear to be described by a boundary layer approach. The extent of macrosegregation was independently confirmed by saturation magnetization measurements, Fig. 16, and suggests that no unusual phases occur during directional solidification processing (e.g., metastable phase formation). The actual eutectic composition probably exists near 8.0 a/o Sm based on the composition and magnetization of the last fraction to solidify. Recent differential thermal analysis of cast samples near this composition region also suggests a lower Sm composition for the eutectic (Ref. 22). Hence our nominal, "eutectic" starting composition was ~ 1 a/o Sm-rich.

Quantitative (least-square fit), primary dendrite diameter and spacing, near the 9 a/o Sm composition region of each sample, revealed the usual dependence of $V^{1/2}$ as shown in Fig. 17. The primary interdendritic spacing, λ_D , varied from ~ 200 μ m at $V = 45.4$ cm/h to ~ 600 μ m at $V = 2.7$ cm/h while



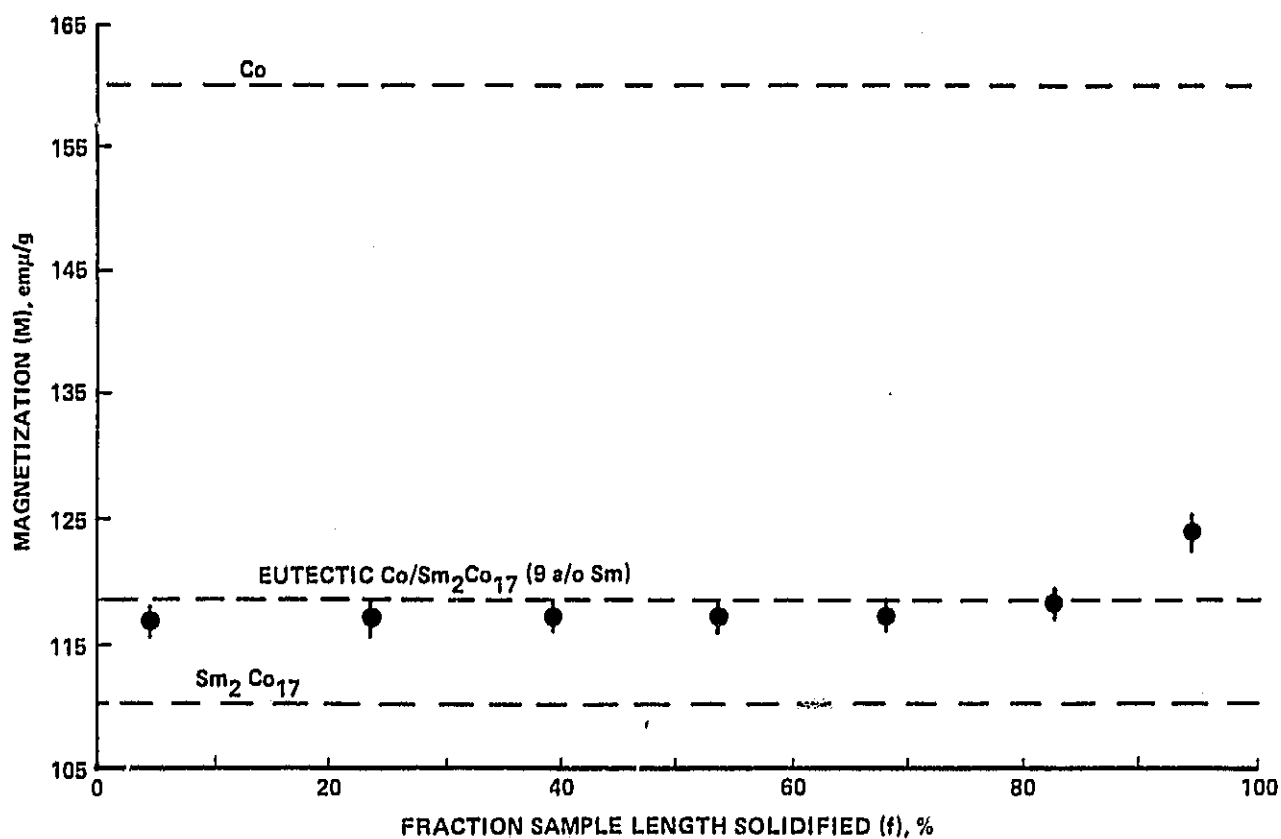
R84-1309-014(T)

Fig. 14 (a) Classical morphological stability G/V criteria necessary for stable, cooperative growth and (b) solidification velocity (critical velocity) necessary for G/V criteria assuming $G_L = 60^\circ\text{C/cm}$



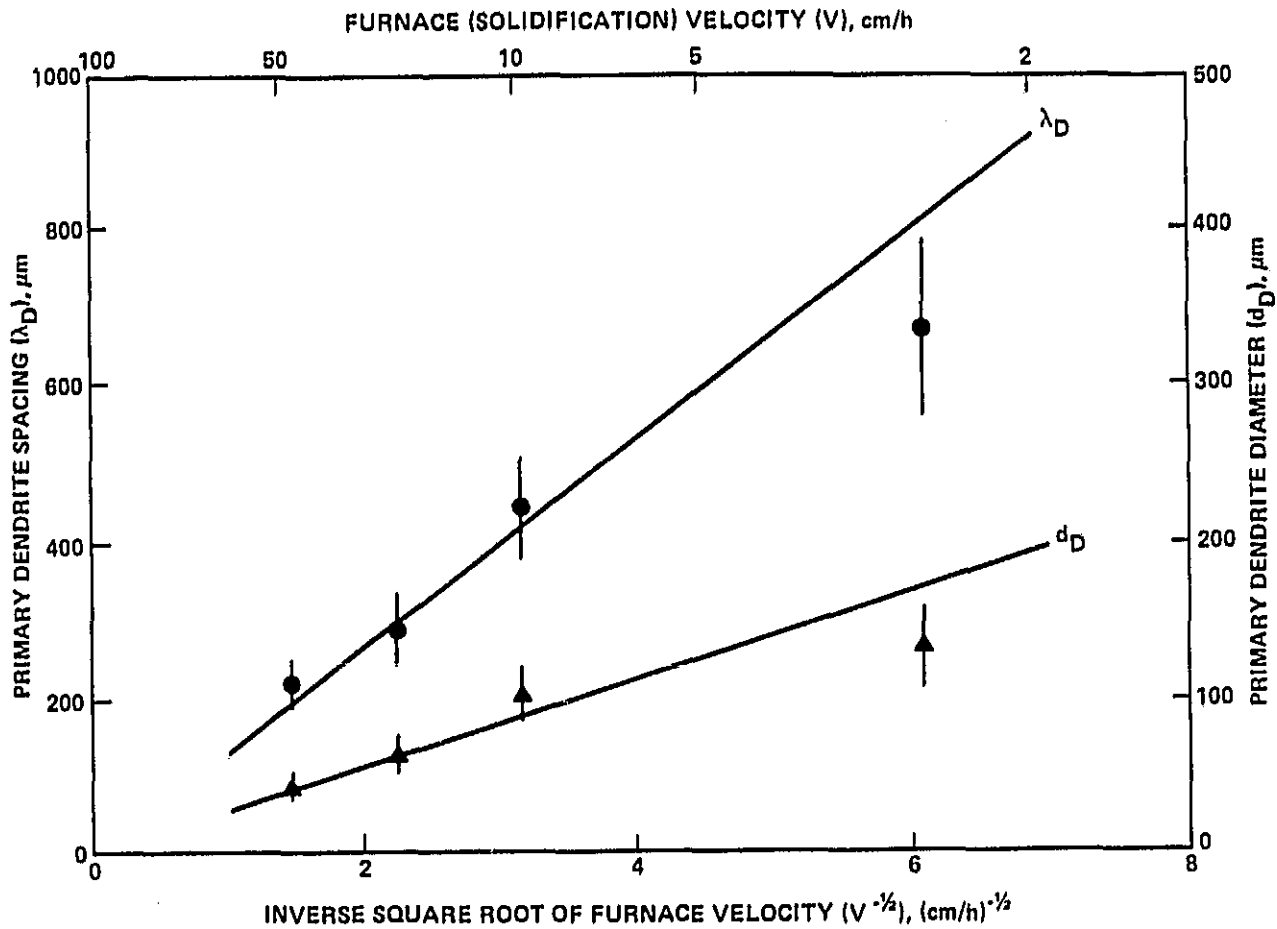
R84-1309-015(T)

Fig. 15 Average composition of Sm in solid for initial composition $C_0 = 9.0$ a/o Sm directionally solidified at $V = 45.4$ cm/h. Curve is best X_2 - fit using Verhoeven model for off-eutectic, cooperative growth



R84-1309-016(T)

Fig. 16 Magnetization (at $H = 200$ kG) parallel to solidification direction as a function of sample length solidified. Superimposed are saturation magnetization values for $\text{Sm}_2\text{Co}_{17}$, theoretical value for 9 a/o Sm and Co. Sample's initial composition was 9 a/o Sm and was directionally solidified at $V = 45.4$ cm/h.



R84-1309-017(T)

Fig. 17 Primary Co dendrite spacing (λ_D) and diameter (d_D), measured transverse to solidification direction, for near $\text{Sm}_2\text{Co}_{17}/\text{Co}$ eutectic composition (9 a/o Sm) as a function of inverse square root of furnace (solidification) velocity. Straight lines are least squares fit to higher furnace velocity data.

the primary dendrite diameter, d_D , changed from $\sim 50 \mu\text{m}$ at 45.4 cm/h to $\sim 200 \mu\text{m}$ at $V = 2.7 \text{ cm/h}$. At the lower solidification velocities, an apparent deviation from the $V^{1/2}$ dependence was found for both λ_D and d_D . Similar behavior has been observed for primary dendrite spacing during aligned directional solidification of Au-Pb and Pb-Sn alloys (Refs. 23 and 24). Temperature gradient induced solute migration and natural convective flow in the interdendritic liquid have been suggested as possible explanations for this deviation. The modeling of the extent of deviation might provide a direct measure of the degree and geometry of convective fluid flow present during solidification of near eutectic $\text{Sm}_2\text{Co}_{17}/\text{Co}$ alloys.

$\text{SmCo}_5/\text{Sm}_2\text{Co}_{17}$ Peritectic

The morphology of directionally solidified $\text{SmCo}_5/\text{Sm}_2\text{Co}_{17}$ peritectic ($C_0 = 12 \text{ a/o Sm}$; Fig. 1) resulted in aligned dendrites of SmCo_5 within a faceted $\text{Sm}_2\text{Co}_{17}$ matrix with appreciable $\text{SmCo}_5/\text{Sm}_2\text{Co}_{17}$ interdendrite structure as seen in Fig. 18. Appreciable macrosegregation in Sm composition was observed and increased with decreasing solidification velocity. The faceting of the $\text{Sm}_2\text{Co}_{17}$ phase was unexpected in view of the results of the $\text{Sm}_2\text{Co}_{17}/\text{Co}$ eutectic and might be related to interfacial undercooling effects during solidification. However, no evidence of coupled peritectic growth was observed in agreement with previous work on the directional solidification of peritectics (Refs. 13 and 14). Clearly, considerably more work dealing with parametric studies of the effects of V , G_L and composition on the growth mechanism must be performed.

Kerr effect microscopy, Fig. 19, demonstrated strip-like magnetic domains in the SmCo_5 primary dendrites transverse to the solidification direction and an irregular domain pattern within the interdendritic, $\text{SmCo}_5/\text{Sm}_2\text{Co}_{17}$ regions. Even though these results are preliminary, they do demonstrate the potential of using the Kerr effect to quantitatively study the crystallographic nature (geometry of domains), magnetocrystalline anisotropy (size of individual domains) and the interface region between magnetic phases (reverse domain nucleation) for this system.

Certain composition segments, corresponding to the $\text{Sm}_2\text{Co}_{17}$ stoichiometry ($\sim 10.5 \text{ a/o Sm}$), were analyzed from a zero remanent magnetization state

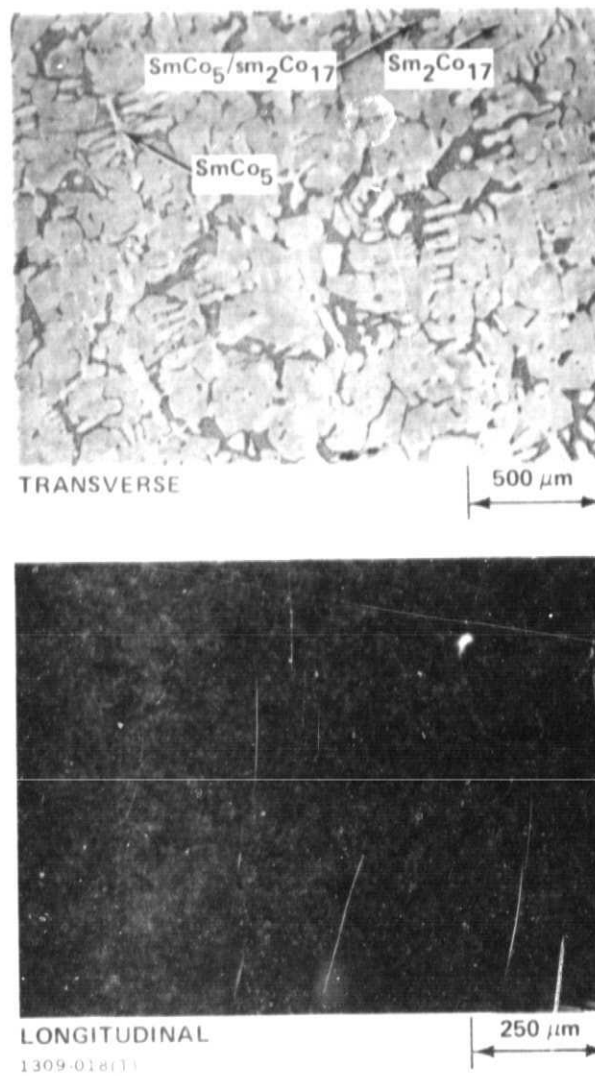
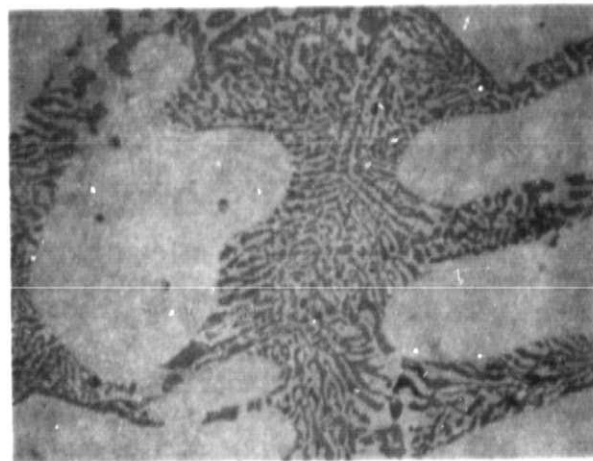


Fig. 18 Morphology transverse and longitudinal to solidification direction for initial composition $C_0 = 12.0$ a/o Sm ($\text{SmCo}_5/\text{Sm}_2\text{Co}_{17}$) directionally solidified at $V = 10$ cm/h



(a)

100 μm



(b)

50 μm

1309-019(T)

Fig. 19 Magnetic domain pattern observed by Kerr effect in (a) ferromagnetic SmCo_5 dendrites and (b) interdendritic $\text{SmCo}_5/\text{Sm}_2\text{Co}_{17}$ structure transverse to solidification direction for peritectic ($C_0 \sim 12.0$ a/o Sm) composition directionally solidified at $V = 10$ cm/h

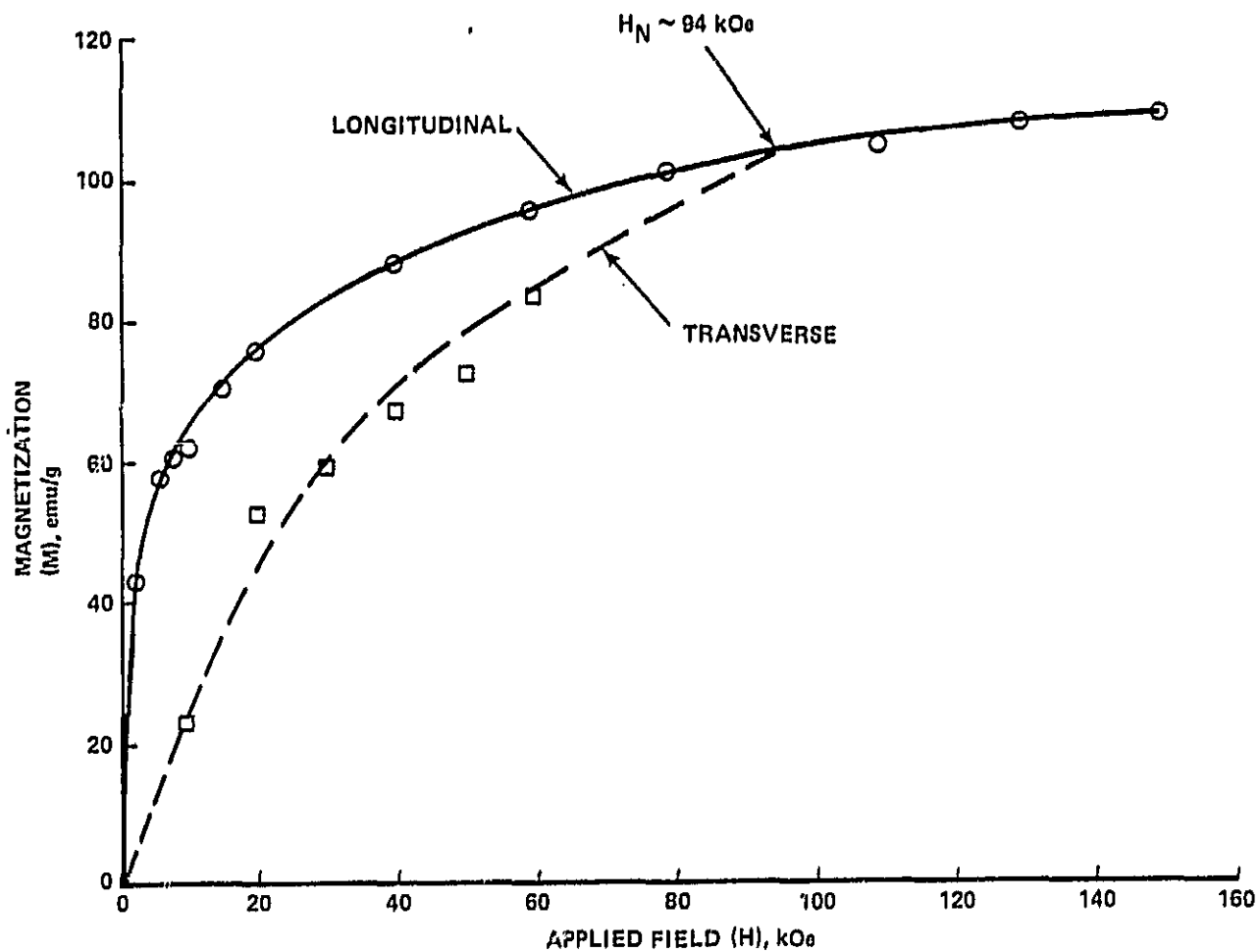
(demagnetized) by measuring their initial magnetization behavior both parallel (longitudinal) and perpendicular (transverse) to the solidification direction. As shown in Fig. 20, there was a clear anisotropy in magnetization with the easy axis of magnetization lying approximately along the direction of solidification (longitudinal). The applied field necessary to remove the anisotropy (nucleation or crystal field, H_N) was found to be ~ 90 kOe which is consistent with previous studies of single crystal $\text{Sm}_2\text{Co}_{17}$ (Ref. 25).

Magnetization, at room temperature, parallel to the solidification direction (easy axis of magnetization), showed the anticipated poor permanent magnet performance (large scale of ferromagnetic phases). As seen in Fig. 21, both near eutectic (8.8 a/o Sm) and peritectic (12 a/o Sm) samples exhibited low magnetic remanence (~ 21 emu/g or $4\pi M = 2200$ kG) and resistance to demagnetization (between 300 and 500 Oe). Since the scale of ferromagnetic phases should be an order of magnitude smaller in coupled, cooperative growth compared with dendritic solidification (Ref. 26; Figs. 12 and 13), significantly improved magnetic performance is anticipated.

Al-Mn System

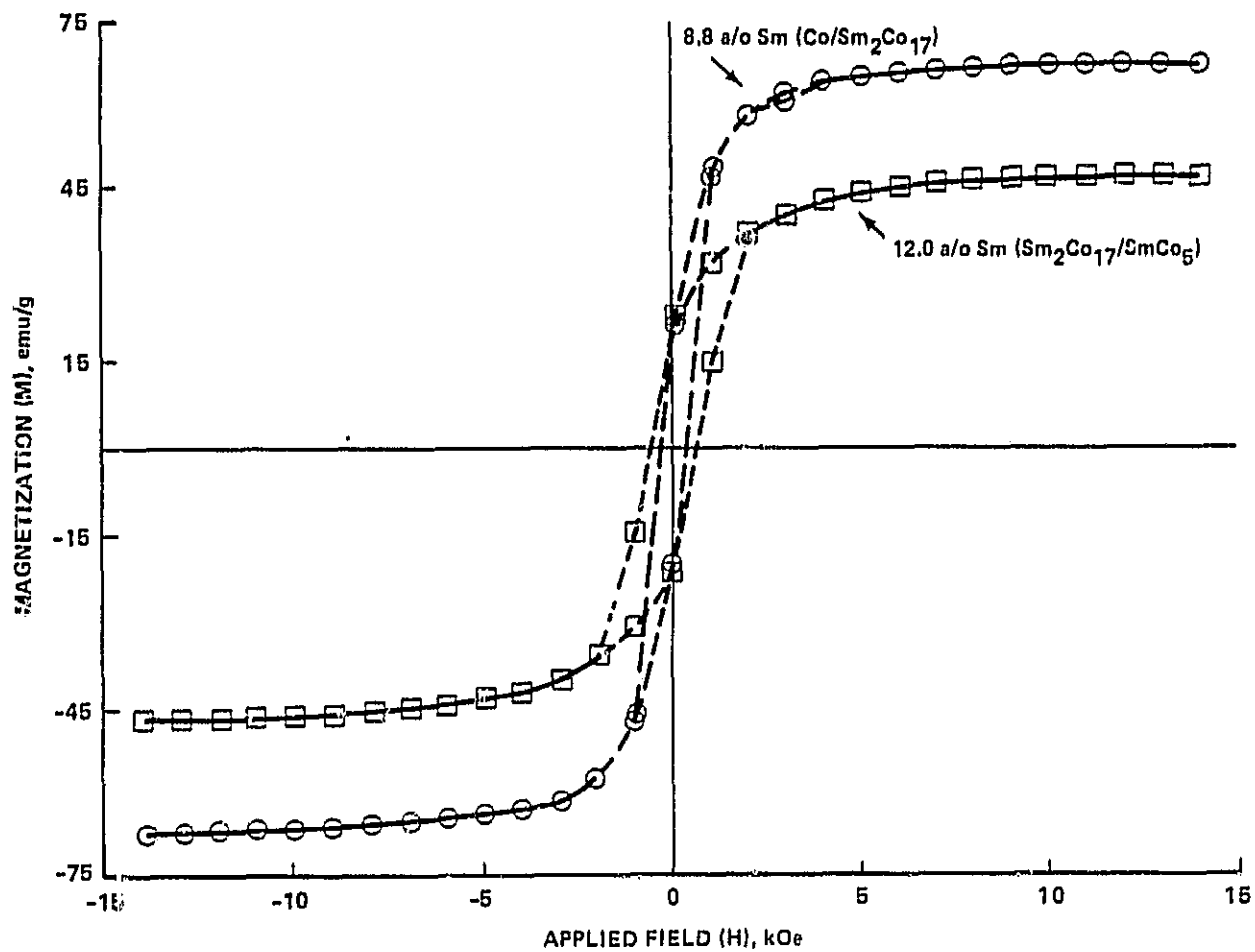
As shown in Fig. 22, the microstructure of a directionally solidified ($V = 0.8$ cm/h and $G \sim 55$ °C/cm) Al-Mn alloy, initially containing ~ 55 a/o Mn, is characterized, in the initial region to solidify, by a two phase structure consisting of randomly oriented Al-rich fibers dispersed in a textureless matrix whose composition is ~ 50 a/o Al, as determined by energy dispersive x-ray analysis. In view of extensive studies of the phase formation and transformation in this composition region of the Al-Mn system (Ref. 20; Fig. 3), we interpret the matrix phase as corresponding to the metastable and magnetically desirous ferrimagnetic τ -phase and the Al-rich fibers as a precipitated Cr_5Al_8 -type Al-Mn phase which presumably forms in the solid state during cooling after solidification. The remaining fraction solidified region of this sample was rich in other peritectic phases such as MnAl_5 , MnAl_4 , etc. (Ref. 27) but these phases were not considered further due to their non-ferromagnetic state.

As seen in Fig. 23, significant macrosegregation was observed for the thermally stable, growth-up (antiparallel to the direction of gravity)



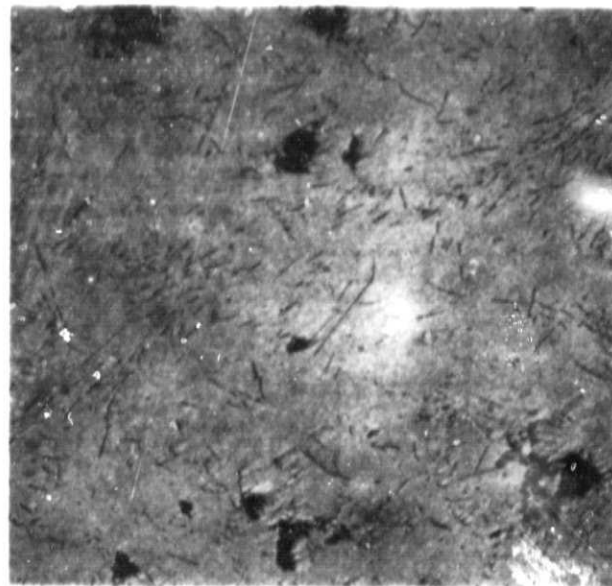
1309-020(T)

Fig. 20 Initial magnetization longitudinal (parallel) and transverse (perpendicular) to solidification direction for sample segment containing ~ 10.5 a/o Sm ($\sim \text{Sm}_2\text{Co}_{17}$). Observed anisotropy is consistent with easy axis of magnetization parallel to solidification direction



1309-021(T)

Fig. 21 Magnetization per unit mass measured at room temperature parallel to solidification direction for near-eutectic (8.8 a/o Sm) and peritectic (12 a/o Sm) compositions



TRANSVERSE

250 μm

Cr_5Al_8 - TYPE

τ - TYPE

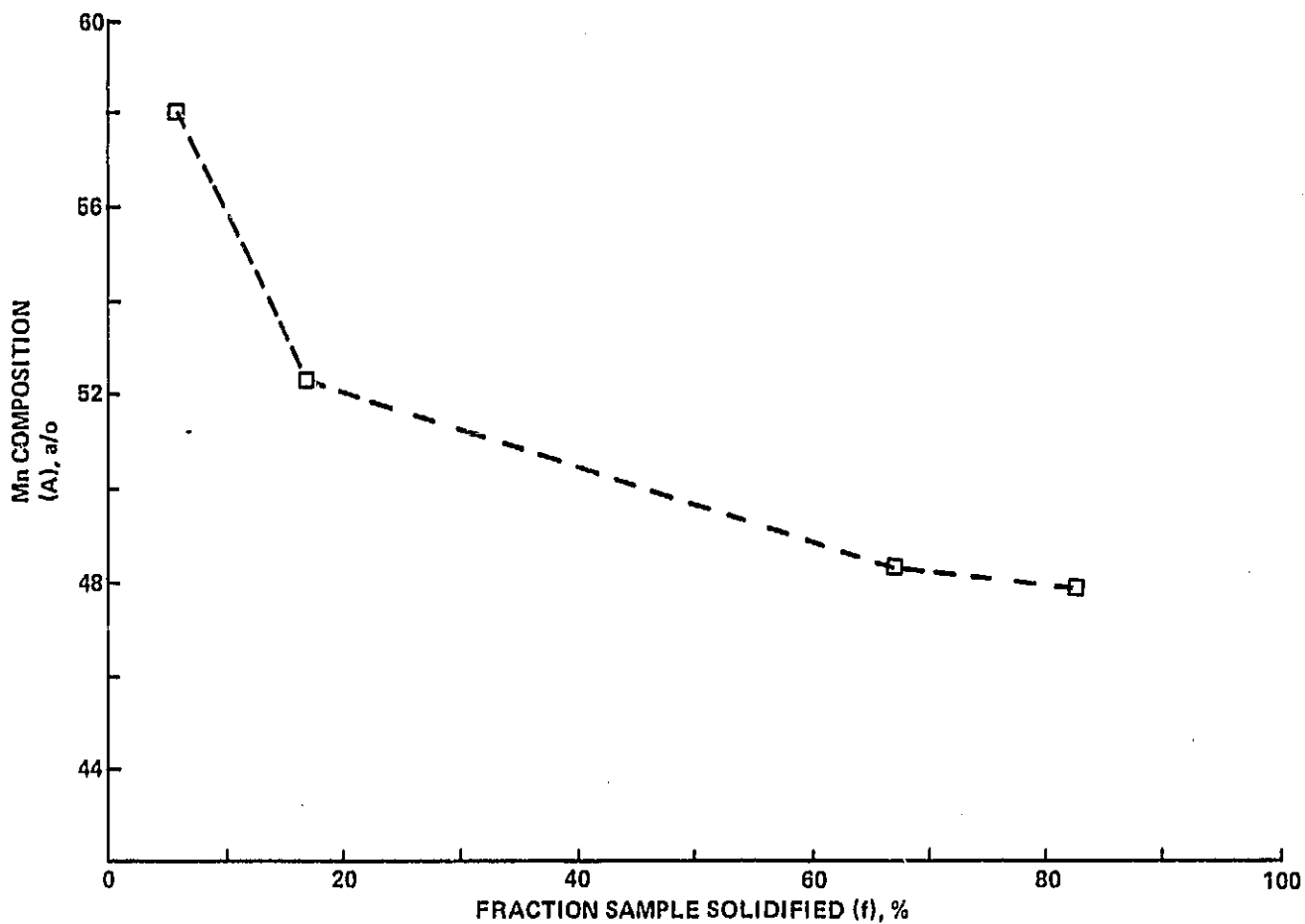


SOLIDIFICATION
DIRECTION (LONGITUDINAL)

50 μm

1309-022(T)

Fig. 22 Selected region of directionally solidified Al-Mn alloy containing ~ 50 a/o Mn both transverse and longitudinal to solidification direction and grown at $V = 10$ cm/h



1309-023(T)

Fig. 23 Measured (wet chemical analysis) bulk, longitudinal macrosegregation for Al-Mn sample containing initially ~ 55 a/o Mn and directionally solidified growth-up at $V = 10$ cm/h and $G \sim 55^\circ\text{C/cm}$

orientation, even at a growth velocity of $V = 10$ cm/h. This segregation might be indicative of appreciable solutally driven convection since the density of Al is only ~50% that of Mn near the solidification temperatures for this range of compositions (Ref. 19). The manifestation of this macrosegregation was most pronounced on the resultant magnetic properties as shown in Figs. 24-26.

Figure 24 shows the initial magnetization curves for the sample whose composition (by wet chemical analysis) versus fraction length solidified is shown in Fig. 23, i.e., directionally solidified at $V = 10$ cm/h with an initial bulk composition ~55 a/o Mn. The ferromagnetic, high magnetization behavior is evident for the initial length to be solidified, percent length $f \leq 20\%$, and is paramagnetic-like for $f > 20\%$, i.e. straightline, Brillouin-like with lower magnetization. In Fig. 25, the abrupt change in magnetization for the same sample shown in Figs. 23 and 24, demonstrates the abrupt transition from the ordered, ferrimagnetic state corresponding to the τ -MnAl phase to the paramagnetic $MnAl_5$ phase. It is interesting to note that the ferrimagnetic τ -phase appears to form directly as a consequence of directional solidification processing rather than requiring additional post-processing heat treatment (Ref. 20) which leads to the sequence of solid-state reactions thought to result in τ -phase formation (Fig. 3). Shown in Fig. 26 is the degree of magnetic anisotropy, i.e., the ratio of magnetization at 14 kOe measured parallel (longitudinal) and perpendicular (transverse) to the solidification direction, observed for three solidification velocities of $V = 0.8, 10$ and 39.9 cm/h. Figure 26 includes the initial sample lengths solidified ($f < 25\%$), where appreciable τ -MnAl phase forms. As seen in Fig. 26, no appreciable anisotropy is apparent suggesting random, isotropic crystallographic orientation for the τ -phase formed during directional solidification for $V = 0.8$ to 39.9 cm/h. However, as shown in Fig. 27, significantly more macrosegregation, i.e. more paramagnetic behavior, less τ -phase and faster transition to non-ferrimagnetic behavior, is observed at $V = 10$ cm/h than $V = 39.9$ cm/h.

It has been previously demonstrated (Refs. 28-29) that annealing of quenched $Mn_{55}Al_{45}$ alloys can lead to enhanced magnetic performance if annealed below $\sim 600^\circ\text{C}$. Supposedly, the anneal results in further conversion of the

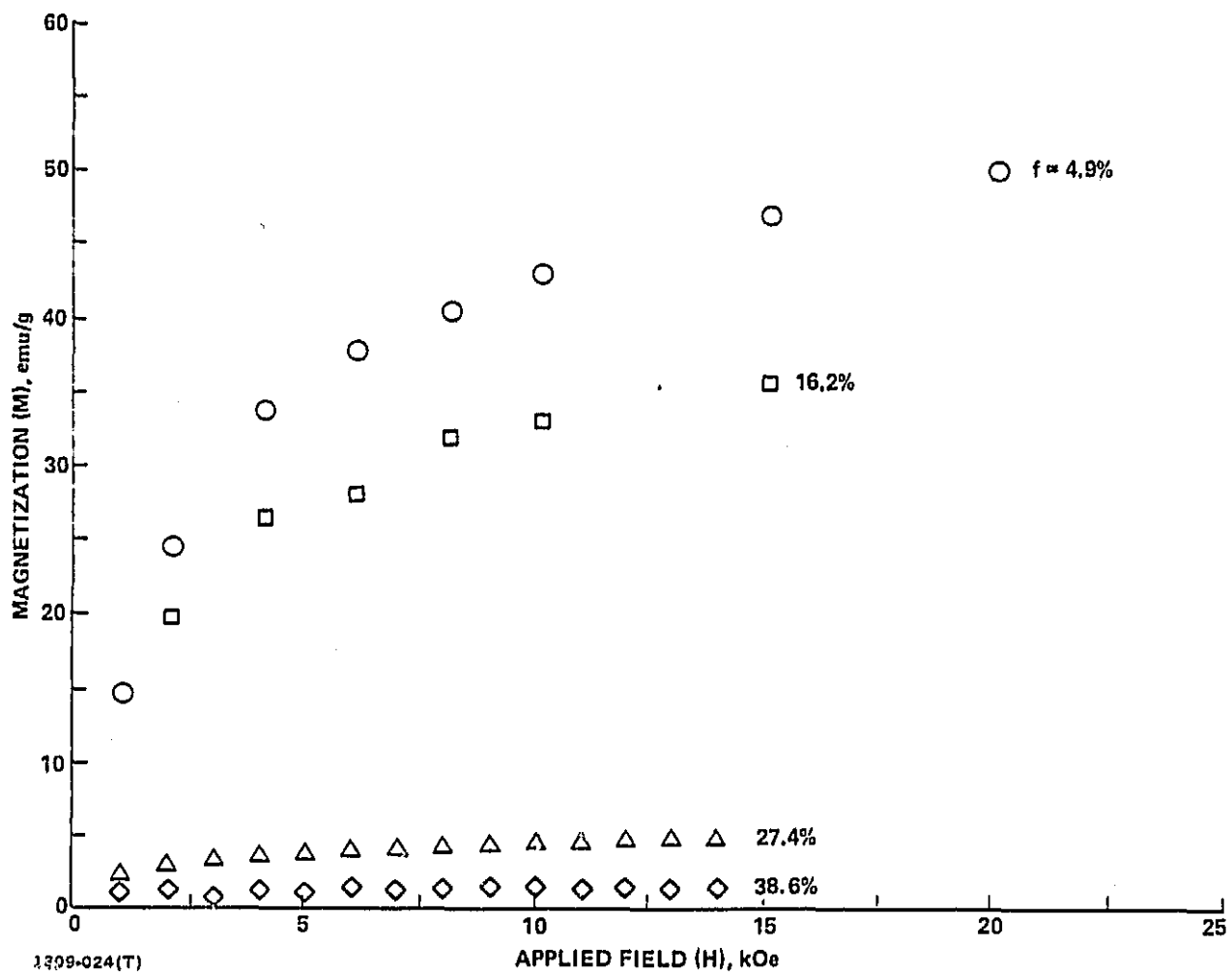


Fig. 24 Initial magnetization measured parallel to the solidification direction as a function of fraction solidified (f) for sample displayed in Fig. 23

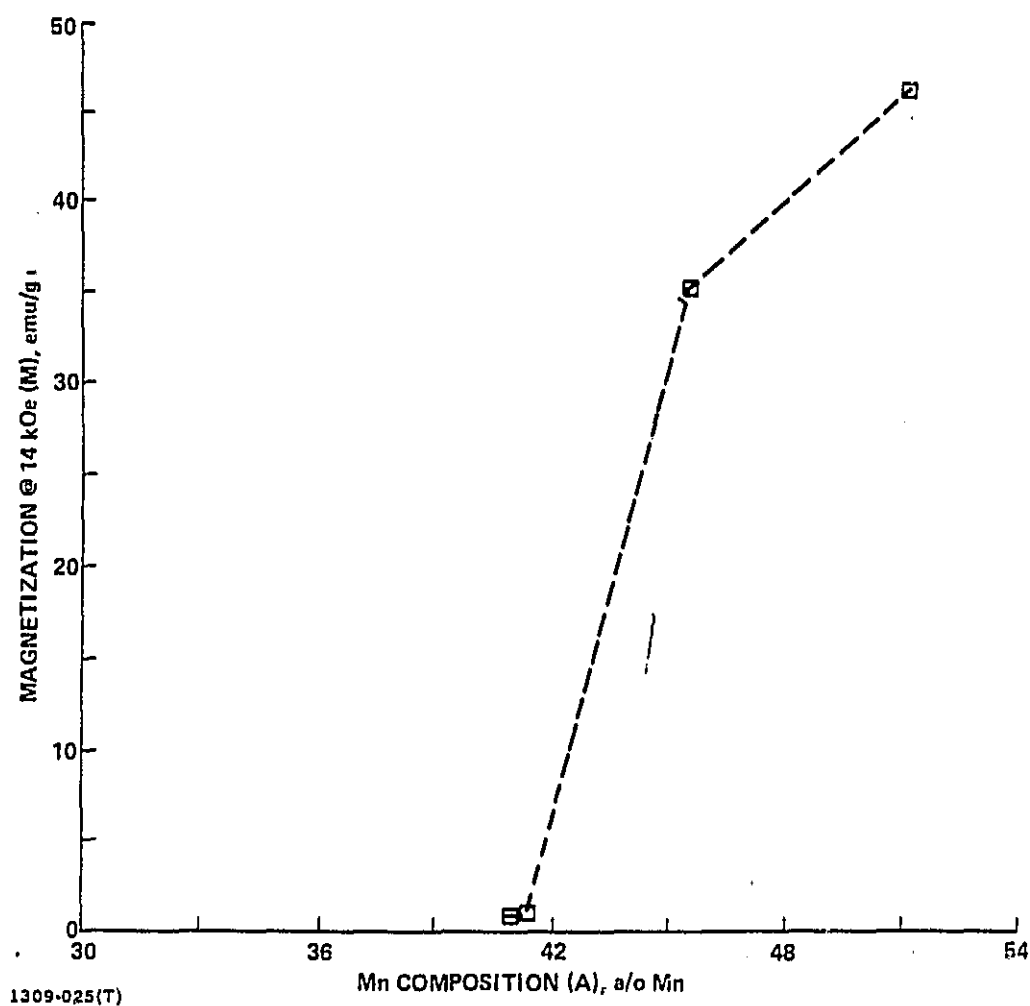


Fig. 25 Magnetization in an applied magnetic field of 14 kOe measured parallel to the solidification direction versus Mn concentration for sample displayed in Figs. 23 and 24

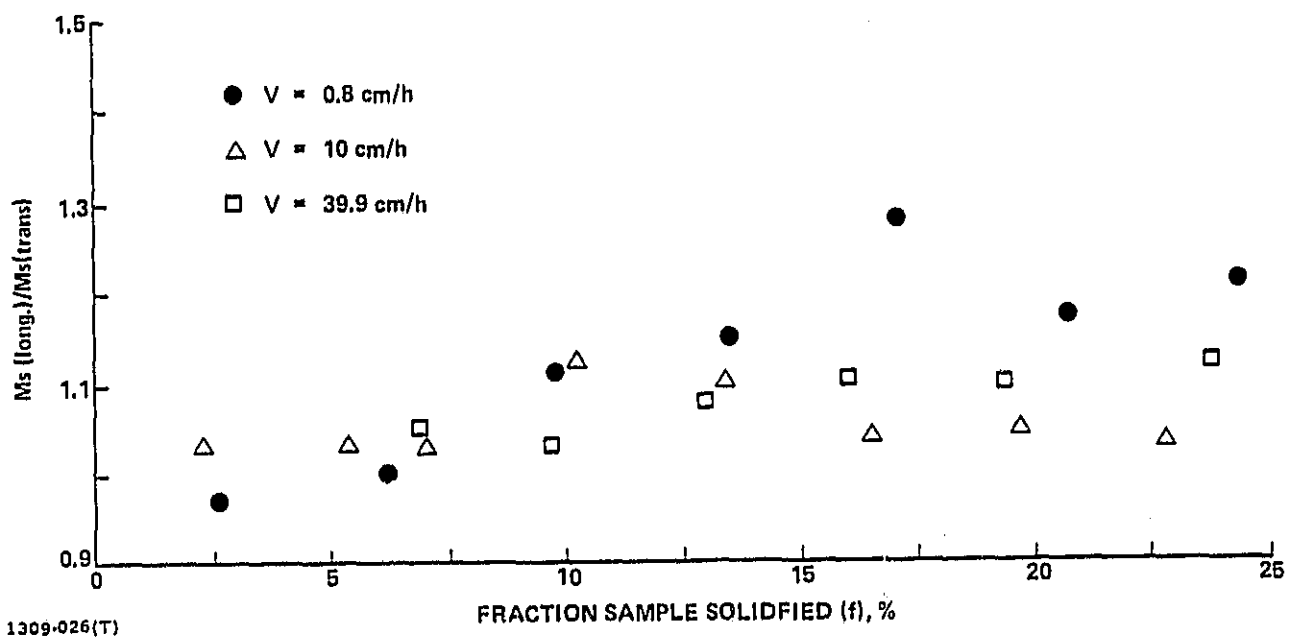
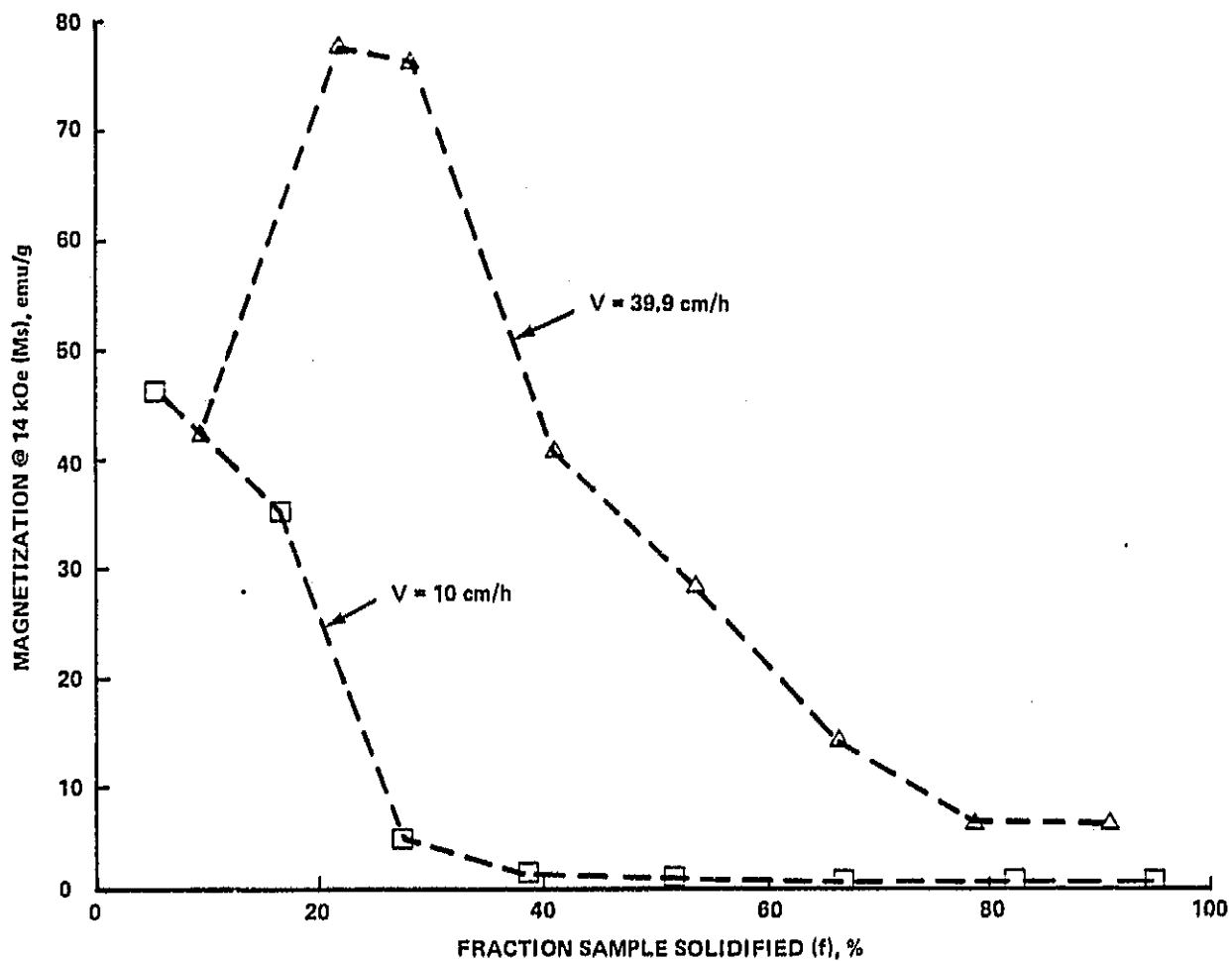


Fig. 26 Ratio of magnetization measured parallel (long.) and perpendicular (trans.) to the solidification direction at an applied magnetic field of 14 kOe for fraction solidified ($f \leq 25\%$) regions containing γ -phase



1309-027(T)

Fig. 27 Magnetization measured parallel to the solidification direction at 14 kOe versus fraction sample length solidified for samples initially containing ~ 55 a/o Mn and directionally solidified at $V = 10$ and 39.9 cm/h with $G \sim 55^\circ\text{C}/\text{cm}$.

hexagonal phase to the desired τ -phase (see Fig. 3). In directionally solidified material, we found initially complete conversion to the τ -phase and, in fact, evidence for solid state precipitation of the Cr_5Al_8 -type MnAl phase (Fig. 22). In order to further investigate this conversion and assess its affect on bulk magnetic properties, selected samples ($V = 10 \text{ cm/h}$; Fig. 23) were heat treated $\sim 800^\circ\text{C}$ for 1 h in an argon atmosphere (in order to provide faster precipitation kinetics) and the resultant microstructure and magnetic properties analyzed.

As seen in Fig. 28, the post-solidification anneal results in both coarsening of the already precipitated Cr_5Al_8 -type MnAl phase (compare with Fig. 22) and further transformation of τ to Cr_5Al_8 -type MnAl . The coarsening and continued precipitation appears to divide the τ -matrix phase (Fig. 28, transverse to solidification direction) into "cells" approximately $100 \mu\text{m}$ in diameter.

Even though there is now less ferrimagnetic τ -phase, the anneal and subsequent change in microstructure results in increasing remanent magnetization (magnetic flux remaining after removal of magnetizing applied field) and resistance to demagnetization. As shown in Fig. 29, the remanent magnetization increases from 12.1 emu/g to 21.9 emu/g (or $4\pi M = 775 \text{ gauss}$ to 1400 gauss) and the resistance to demagnetization from 660 Oe to 1150 Oe .

These improved properties may be due to enhanced domain wall pinning which occurs at the inhomogeneous magnetic surfaces between the τ -matrix and Cr_5Al_8 -type MnAl phase boundaries. As displayed in Fig. 30, the resultant hysteresis curve of the heat treated sample gives rise to a maximum static energy product (related to magnetic potential energy) of $(BH)_{\text{max}} = 3 \times 10^5 \text{ G-Oe}$. Also evident in Fig. 30 is the approach to saturation and non-square hysteresis loop shape which is characteristic of random orientation of the easy axis of magnetization. If preferred crystallographic orientation could be achieved through greater solidification control, energy products 40 times greater would be anticipated.

ORIGINAL PHOTOGRAPH
OF POOR QUALITY

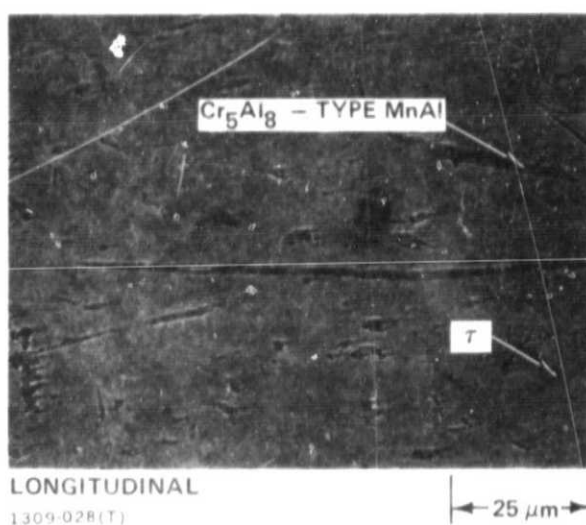
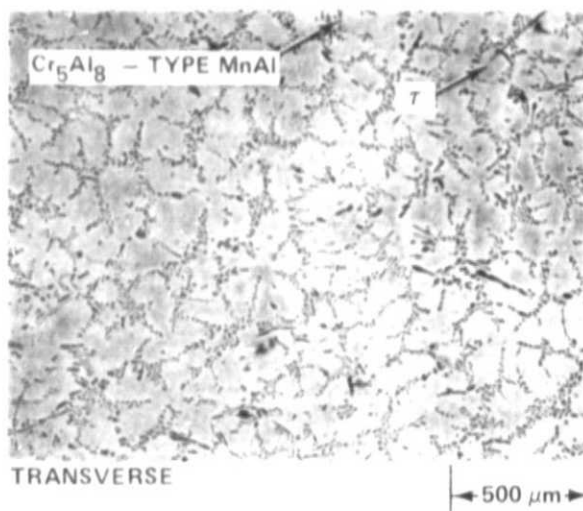
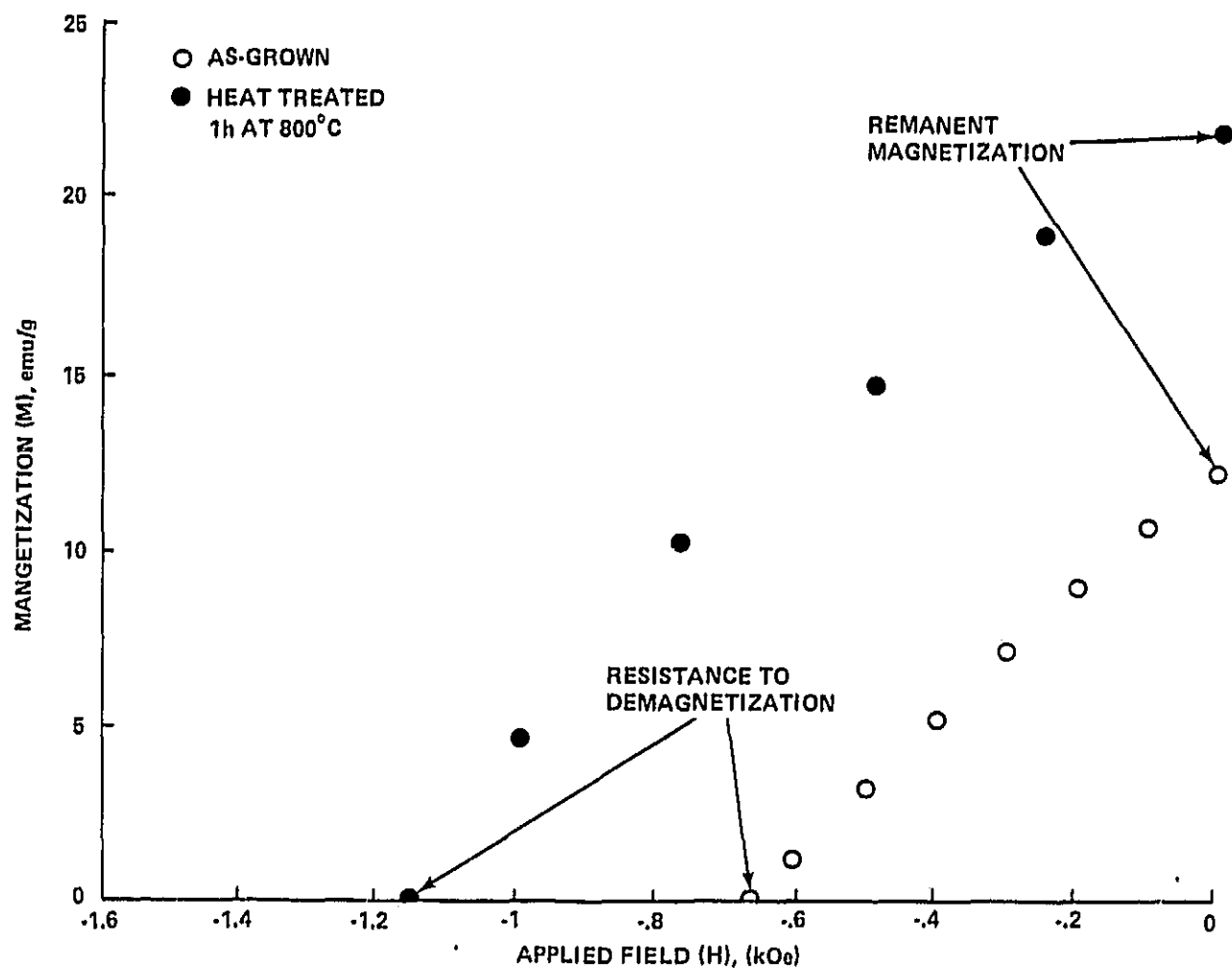
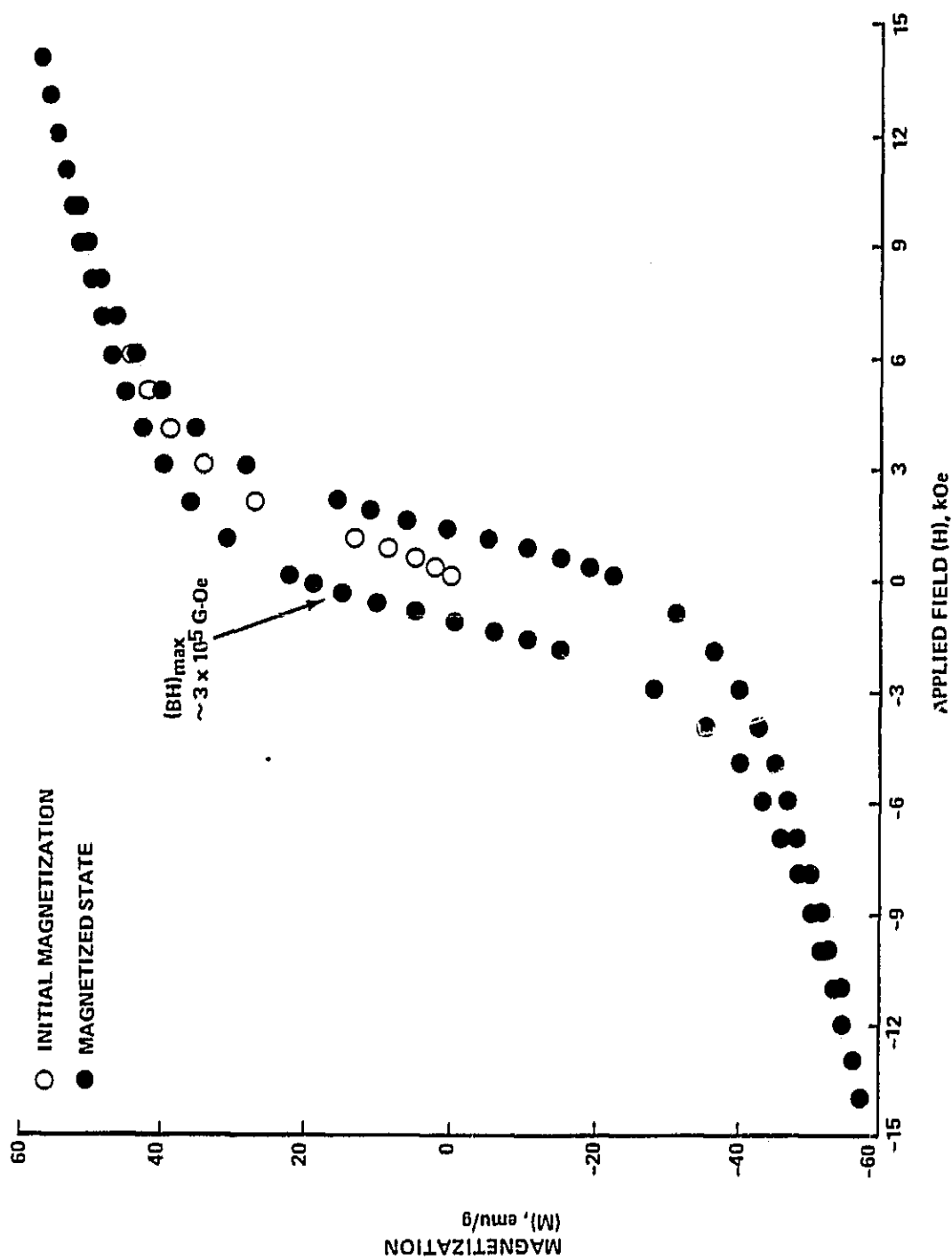


Fig. 28 Selected region of directionally solidified Al-Mn alloy grown at $V = 10$ cm/h and heat treated 1 h at 800°C in argon atmosphere. Sample segment composition is ~ 50 a/o Mn



1309-029(T)

Fig. 29 Demagnetization behavior of directionally solidified Al-Mn alloy segment containing ~ 50 a/o Mn measured parallel to the solidification direction in as-grown and post heat treated states.



1309-030(T)

Fig. 30 Initial magnetization and hysteresis curve for heat treated Al-Mn segment containing ~ 50 a/o Mn and measured parallel to solidification direction

SUMMARY AND FUTURE EXPERIMENTS

An investigation conducted to characterize the effects of directional solidification on the microstructural, compositional and magnetic properties of the commercially important Co-Sm and Al-Mn systems has:

- o Demonstrated a lower Sm-composition (~8 a/o Sm compared with 9 a/o Sm) for the $\text{Sm}_2\text{Co}_{17}/\text{Co}$ eutectic
- o Established that for small variations from the $\text{Sm}_2\text{Co}_{17}/\text{Co}$ eutectic composition, dendritic rather than cooperative growth is preferred
- o Determined that lamellar-like eutectic, cooperative growth for the eutectic $\text{Sm}_2\text{Co}_{17}/\text{Co}$ may be possible for higher G/V values and a eutectic starting composition
- o Demonstrated aligned dendritic growth, for both near $\text{Sm}_2\text{Co}_{17}/\text{Co}$ eutectic and $\text{SmCo}_5/\text{Sm}_2\text{Co}_{17}$ peritectic, with the desired easy axis of magnetization lying parallel to the direction of solidification
- o Established that no unusual "metastable" phases form from peritectic compounds of the Co-Sm system and that dendritic rather than cooperative growth occurs over the range of processing conditions used
- o Established that natural convection occurs during directional solidification of near eutectic $\text{Sm}_2\text{Co}_{17}/\text{Co}$, peritectic $\text{SmCo}_5/\text{Sm}_2\text{Co}_{17}$ and $\text{M}_{55}\text{Al}_{45}$ alloys resulting in high levels of macrosegregation
- o Determined that appreciable, ferrimagnetic $\tau\text{-MnAl}$ forms as a consequence of Bridgman-Stockbarger directional solidification without post-solidification annealing
- o Demonstrated isotropic, polycrystalline growth for peritectic Al-Mn alloys over the range of directional solidification conditions studied

PRECEDING PAGE BLANK NOT FILMED

ACKNOWLEDGEMENTS

The author would like to thank G. Busch, R. Lange and W. Poit of Grumman for sample preparation and magnetic, microstructural and electron microscopy measurements; Dr. D.J. Larson, Jr. of Grumman for helpful discussions concerning the Bi-Pb and eutectic Co-Sm systems; Prof. M. Glicksman of Rensselaer Polytechnic Institute for his insight and helpful suggestions regarding dendritic solidification; Dr. B. Brandt, Dr. S. Foner, E. McNiff and L. Rubin of the Francis Bitter National Magnet Laboratory for their technical assistance in performing high magnetic field measurements and Drs. P. Adler and R. DeIasi of Grumman for their critical reading of this manuscript and helpful suggestions.

PRECEDING PAGE BLANK NOT FILMED

REFERENCES

1. E. Nesbitt and J. Wernick, "Rare Earth Permanent Magnets", Academic Press, New York, NY, 1973.
2. H. Senno and Y. Tawara, Japan J. Appl. Phys., Vol. 14, p. 1619, 1975.
3. J. Croat, J. Herbst, R. Lee and F. Pinkerton, General Motors Research Laboratories Publication GMR-4492, General Motors Corp., Warren, MI, 1983.
4. J. Van den Broek and J. Van Landuyt, Acta Metallurgica, Vol. 27, p. 1497, 1979.
5. T. Ojima, S. Tomizawa, T. Yonezawa and T. Hori, IEEE Trans. Mag., Vol. MAG-13, p. 1317, 1977.
6. H. Kronmuller, Proc. Third Intl. Workshop on Rare Earth-Cobalt Permanent Magnets and Their Applications, Vol. 2, p. 1, San Diego, CA, 1978.
7. R. Glardon and W. Kurz, Proc. Third Intl. Workshop on Rare Earth-Cobalt Permanent Magnets and Their Applications, Vol. 1, p. 504, San Diego, CA, 1978.
8. M. Notis, D. Shah, S. Young and C. Graham, IEEE Trans. Mag., Vol. MAG-15, p. 957, 1979.
9. R. Pirich and D. Larson, J. Appl. Phys., Vol. 50, p. 2425, 1979.
10. F. Cadieu, S. Aly, T. Cheung and R. Pirich, J. Appl. Phys., Vol. 53, p. 2401, 1982.
11. R. Pirich, D. Larson and G. Busch, IEEE Trans. Mag., Vol. MAG-15, p. 1754, 1979.
12. R. Pirich, IEEE Trans. Mag., Vol. MAG-16, p. 1065, 1980.
13. G. Scherbakov, S. David and M. Brody, Scripta Met., Vol. 8, p. 1239, 1974.
14. W. Boettinger, Met. Trans. A, Vol. 5, p. 2023, 1974.
15. D. Larson and R. Pirich, Grumman Research and Development Center Memorandum RM-714, Grumman Aerospace Corporation, Bethpage, NY, 1981.
16. T. Fu and W. Wilcox, J. Crys. Growth, Vol. 51, p. 557, 1981.
17. R. Pirich, D. Larson and G. Busch, AIAA Jnl., Vol. 19, p. 589, 1981.
18. E. Nesbitt, "Ferromagnetic Domains - A Basic Approach to the Study of Magnetism", Bell Telephone Laboratory, Murray Hill, NJ, 1962.
19. K.H.J. Buschow and A.S. Van der Goot, J. Less Common Metals, Vol. 14, p. 323, 1968.

20. J.J. Van de Broek and H. Donkersloot, Acta Metallurgica, Vol. 27, p. 1497, 1979.
21. J.D. Verhoeven and R.H. Homer, J. Crys. Growth, Vol. 1, p. 3437, 1970
22. D.J. Larson, Jr., private communications.
23. C.M. Klaren, J.D. Verhoeven and R. Trivedi, Met. Trans. A., Vol. 11A, p. 1853, 1980.
24. J.T. Mason, J.D. Verhoeven and R. Trivedi, Ames Laboratory Report IS-3720, Ames, IA, 1981.
25. R.S. Perkins, S. Gaiffi and A. Menth, IEEE Trans. Mag., Vol. MAG-11, p. 1431, 1975.
26. M.C. Flemings, "Solidification Processing," McGraw-Hill, New York, NY 1974.
27. R. Hultgren, P.D. Desai, D.T. Hawkins, M. Gleiser and K.K. Kelley, "Selected Values of the Thermodynamic Properties of Binary Alloys," American Society for Metals, Ohio, 1973.
28. A.J.J. Koch, P. Hokkelling, M.G. Van den Steeg and K.J. de Vos, J. Appl. Phys., Vol. 31, p. 775, 1960.
29. T. Ohtani, N. Kato, S. Kohima, Y. Sakamoto, I. Konno, M. Tsukahara and T. Kubo, IEEE Trans. Mag., Vol. MAG-13, p. 1328, 1977.

PROGRAM ASSOCIATED PUBLICATIONS & PRESENTATIONS

- o R. Pirich "The Effects of Gravity During Directional Solidification of Ferromagnetic Composites", Invited Colloquim, Queens College of CUNY, Queens, NY, 1981.
- o R. Pirich, "Permanent Magnet Composite Materials", Annual Report of the Francis Bitter National Laboratory, MIT Press, Cambridge, MA, 1982.
- o R. Pirich, "Phase Formation and Transformation of High Anisotropy Ferromagnetic Compounds," Invited Seminar, Physics Dept., Adelphi University, Garden City, NY, 1983.